UNCLASSIFIED

AD NUMBER

AD337619

CLASSIFICATION CHANGES

TO: unclassified

FROM: confidential

LIMITATION CHANGES

TO:

Approved for public release, distribution unlimited

FROM:

Distribution authorized to DoD only; Administrative/Operational Use; Jul 1963. Other requests shall be referred to the Arnold Engineering Development Center, Arnold AFS, TN.

AUTHORITY

AEDC USAF ltr, 25 Jul 1969; AEDC USAF ltr, 25 Jul 1969

THIS PAGE IS UNCLASSIFIED

DECLASSIFIED / UNCLASSIFIED
[redacted]

AEDC-TDR-63-100

ARO, INC.
DOCUMENT CONTROL
NO IG-377-343
COPY 17 OF 30
SERIES A PAGES 60

ARCHIVE COPY
DO NOT LOAN

(TITLE UNCLASSIFIED)

PRESSURE AND HEAT-TRANSFER DISTRIBUTIONS ON EXIT AND RE-ENTRY CONFIGURATIONS OF THE GEMINI SPACECRAFT AT MACH NUMBER 8 AND 10

By

O. R. Pritts and G. H. Merz
von Kármán Gas Dynamics Facility
ARO, Inc.

TECHNICAL DOCUMENTARY REPORT NO. AEDC-TDR-63-100

PROPERTY OF U. S. AIR FORCE
AEDC LIBRARY
AF 40(600)1000

July 1963

AFSC Program Area 921E

AEDC TECHNICAL LIBRARY
5 0720 00040 2133

(Prepared under Contract No. AF 40(600)-1000 by ARO, Inc., contract operator of AEDC, Arnold Air Force Station, Tenn.)

This document has been approved for public release and sale; its distribution is unlimited.

ARNOLD ENGINEERING DEVELOPMENT CENTER

AIR FORCE SYSTEMS COMMAND

UNITED STATES AIR FORCE

CLASSIFICATION CANCELLED (CHANGED TO _____)
BY AUTHORITY OF AF letter 8 Apr. 69, signed William O. Cole
Official authorized to change
BY Ed Berg 9 Apr. 69
Name and Position of Individual
[redacted]
DECLASSIFIED / UNCLASSIFIED
[redacted]

NOTICES

Qualified requesters may obtain copies of this report from ASTIA. Orders will be expedited if placed through the librarian or other staff member designated to request and receive documents from ASTIA.

When Government drawings, specifications or other data are used for any purpose other than in connection with a definitely related Government procurement operation, the United States Government thereby incurs no responsibility nor any obligation whatsoever; and the fact that the Government may have formulated, furnished, or in any way supplied the said drawings, specifications, or other data, is not to be regarded by implication or otherwise as in any manner licensing the holder or any other person or corporation, or conveying any rights or permission to manufacture, use, or sell any patented invention that may in any way be related thereto.

This document contains information affecting the national defense of the United States within the meaning of the Espionage Laws (Title 18, U.S.C., sections 793 and 794) the transmission or revelation of which in any manner to an unauthorized person is prohibited by law.

Dissemination outside Department of Defense is prohibited without prior approval of the Gemini Spacecraft Project Office, or AEDC. The use of the data in this report in any other publication is prohibited unless authorized by the Gemini Spacecraft Project Office, NASA Manned Spacecraft Center.

This document has been approved for public release and sale; its distribution is unlimited.
per AF letter, 25 July 69, signed William O. Cole

DECLASSIFIED / UNCLASSIFIED

(Title Unclassified)

PRESSURE AND HEAT-TRANSFER DISTRIBUTIONS ON EXIT AND RE-ENTRY CONFIGURATIONS OF THE GEMINI SPACECRAFT AT MACH NUMBER 8 AND 10

By

O. R. Pritts and G. H. Merz
von Kármán Gas Dynamics Facility
ARO, Inc.
a subsidiary of Sverdrup and Parcel, Inc.

July 1963

ARO Project No. VT1258

CLASSIFICATION CANCELLED (~~CHANGED TO~~.....)
BY AUTHORITY OF AF letter, 9 April 1969, signed William O. Cole
Official authorized to change
BY Ted Boyd 9 April 69
Name and Position of Individual Date

DECLASSIFIED / UNCLASSIFIED

(This abstract is UNCLASSIFIED.)

ABSTRACT

Selected results are presented from heat-transfer and pressure distribution tests of the Gemini exit and re-entry configurations and a hemisphere-cylinder configuration in the hypersonic regime. The effects of configuration, model attitude, and Reynolds number variation on heat-transfer and pressure distributions on the Gemini vehicle were investigated. The tests were conducted at Mach numbers of 8 and 10 and various free-stream Reynolds numbers. The angle-of-attack range was from -40 to 40 deg at selected angles of yaw from 0 to 20 deg.

PUBLICATION REVIEW

This report has been reviewed and publication is approved.

Darreld K Calkins

Darreld K. Calkins
Major, USAF
AF Representative, VKF
DCS/Test

Jean A Jack

Jean A. Jack
Colonel, USAF
DCS/Test

CONTENTS

TABLES

ILLUSTRATIONS

NOMENCLATURE

b	Skin thickness, ft
C_p	Coefficient of pressure
c	Specific heat of model wall material, Btu/lb, °R
D	Diameter, ft
du/ds	Velocity gradient at stagnation point, ft/sec-ft
h	Heat-transfer coefficient, Btu/ft^2-sec-°R
h_{s_t}	Theoretical value of stagnation point heat-transfer coefficient, Btu/ft^2-sec-°R
k	Thermal conductivity of air
M	Mach number
Nu	Correlation Nusselt number, hs D*/k_B
p	Pressure, lb/in.^{2}
q	Rate of heat transfer, Btu/sec-ft^2
R	Model nose radius, ft
Re	Correlation Reynolds number, $\rho_B \frac{du}{ds} D^{*2}/\mu_B$
RE	Free-stream Reynolds number notation, $\rho_\infty V_\infty/\mu_\infty$, per ft
r	Model radius, ft
S	Distance measured from stagnation point, ft
T	Temperature, °R
t	Time, sec
V	Free-stream velocity, ft/sec
w	Density of model wall material, lb/ft^3
α	Angle of attack, deg
μ	Viscosity of air, slugs/ft sec
ρ	Density of air, slugs/ft^3
Φ	Model reference angle, deg (See Figs. 3 and 4)
ϕ	Tunnel roll angle, deg (clockwise looking upstream)
ψ	Angle of yaw, deg

SUPERSCRIPT

*	Evaluated at sonic point

SUBSCRIPTS

B	Evaluated at bulk conditions, $T_B = (T_o + T)/2$
o	Stagnation conditions
t_2	Conditions behind a normal shock
w	Wall conditions
∞	Free-stream conditions

1.0 INTRODUCTION

At the request of the Manned Spacecraft Center (MSC), National Aeronautics and Space Administration (NASA), pressure distribution and heat-transfer tests of 0.10-scale models of the Gemini spacecraft have been conducted for McDonnell Aircraft Corporation (MAC) at nominal Mach numbers of 8 and 10. The tests were performed in the 50-Inch Mach 8 Tunnel (B) and the 50-Inch Mach 10 Tunnel (C) of the von Kármán Gas Dynamics Facility (VKF), Arnold Engineering Development Center (AEDC), Air Force Systems Command (AFSC), intermittently during the period from July 17, 1962, to October 20, 1962. Heat-transfer and pressure distributions were obtained on a hemisphere-cylinder configuration at Mach 10 during the period from January 3 to January 10, 1963.

The launch configuration was tested at free-stream unit Reynolds numbers of 0.63 and 1.35 million per foot, angles of attack from -20 to 20 deg at 0-deg angle of yaw, and angles of yaw from 0 to 20 deg at 0-deg angle of attack in the 50-Inch Mach 8 Tunnel (B). The original configuration with the minus 18-deg canted flat nose and the modified configuration with the 0-deg flat nose were tested at Mach 8 and 10. The heat-transfer tests on the modified launch configuration were performed in the 50-Inch Mach 10 Tunnel (C). Shadowgraphs were obtained for each model attitude and Reynolds number.

The re-entry configuration was tested at free-stream unit Reynolds numbers of 0.72, 1.44, and 2.12 million per foot and angles of attack from -40 to 40 deg in the 50-Inch Mach 10 Tunnel (C). Shadowgraphs were obtained for each model attitude at the high and low Reynolds numbers. Additional heat-transfer data were taken at zero angle of attack at free-stream unit Reynolds numbers of 0.58, 0.83, 1.06, 1.28, 1.51, 1.73, and 1.95 million per foot.

The purpose of the investigation on the hemisphere-cylinder was to obtain heat-transfer and pressure distributions on a basic shape for correlation with the Gemini results and to provide a comparison with theoretical results. Heat-transfer and pressure distribution data were obtained at zero-deg angle of attack and free-stream unit Reynolds numbers from 1.0 to 2.4 million per foot.

The primary objective of the test program was to provide NASA and MAC with aerothermodynamic performance and design data on the Gemini spacecraft.

Manuscript received April 1963.

2.0 APPARATUS

2.1 WIND TUNNELS

The 50-Inch Mach 8 Tunnel (B) and the 50-Inch Mach 10 Tunnel (C) are axisymmetric, continuous flow, variable-density, hypersonic wind tunnels. Because of changes in boundary-layer thicknesses due to changing pressure levels, the Mach 8 and 10 contoured nozzles produce average test section Mach numbers which vary from 8.0 at a stagnation pressure of 100 psia to 8.1 at 900 psia and from 10.0 at a stagnation pressure of 200 psia to 10.2 at 2000 psia, respectively. Details of the tunnels are shown in Figs. 1 and 2.

Stagnation pressures up to approximately 900 psia are supplied to the 50-Inch Mach 8 Tunnel (B) and, 2000 psia to the 50-Inch Mach 10 Tunnel (C) by the VKF 92,500-hp compressor system. The air is selectively valved through the compressor system, high-pressure driers, and propane-fired heater. The gas-fired heater produces a maximum air temperature of 900°F for the 50-Inch Mach 8 Tunnel (B) and preheats the air for the 50-Inch Mach 10 Tunnel (C), which requires the addition of the 12,000-kw electric heater to increase the air temperature to a maximum of 1450°F. These temperatures are sufficient to prevent liquefaction of the air in the corresponding test sections. After heating, the air flows through the nozzle, diffuser, cooler, and back into the compressor system.

A unique feature of the 50-Inch Mach 10 Tunnel (C) is the model installation chamber below the test section which allows the entire pitch mechanism, sting, and model to be lowered out of the tunnel. When the model is in the retracted position, the fairing doors and the safety door can be closed (Fig. 2), and the tank can be entered for model changes while the tunnel is running. When the model is in the test section, only the fairing doors are closed, and the tank remains at tunnel static pressure.

A complete description of the tunnels is given in Ref. 1.

2.2 MODELS

Six models were used in performing wind tunnel tests on the Gemini configurations. Two basic configurations were tested; the launch or exit configuration and the re-entry configuration. Separate heat-transfer and pressure models were fabricated for each configuration. Details of the geometry of the configurations are presented in Figs. 3 and 4.

Pertinent information concerning each model is summarized as follows:

A. Original exit pressure model: material, type 304 stainless steel; fabrication, heavy wall construction; instrumentation, 99 pressure taps formed by welding tubing in model wall and located as shown in Table 2.

B. Modified exit pressure model; same as above except 98 pressure taps were incorporated into this model. Location of these taps is shown in Table 2.

C. Original exit heat-transfer model; material, type 321 stainless steel; fabrication, thin skin construction; instrumentation, 103 chromel-alumel thermocouples welded to the inside surface of the skin. Skin thicknesses and thermocouple locations are presented in Table 2.

D. Modified exit heat-transfer model; same as above except 121 chromel-alumel thermocouples were used. Table 2 shows thermocouple location and skin thickness.

E. Re-entry pressure model; material, type 304 stainless steel; fabrication, heavy wall construction; instrumentation, 99 pressure taps formed by welding tubing in the model wall. Location of these taps is shown in Table 3.

F. Re-entry heat-transfer model; material, type 321 stainless steel; fabrication, thin skin construction; instrumentation, 183 chromel-alumel thermocouples welded to the inside surface of the skin. Skin thicknesses and thermocouple locations are presented in Table 3.

The modified exit configurations were similar to the original models except that the scarf angle on the antenna housing was changed from 18 to 0 deg, and the horizontal scanner was enlarged and relocated (Fig. 3).

The hemisphere-cylinder model was of thin skin construction (nominally 0.030 in.) with the shell fabricated from 310 stainless steel. The model was designed with the body shell thermally insulated from all body support structure with Electrobestos. Details of the model geometry are shown in Fig. 5, and skin thicknesses and instrumentation locations are presented in Table 4.

Photographs of each configuration are presented in Fig. 6.

2.3 INSTRUMENTATION

2.3.1 Pressure Distribution Phase, 50-Inch Mach 10 Tunnel (C)

The pressure data system consists basically of nine channels, each of which is time-shared between eleven model orifices by 12-position Giannini pressure switching valves. The total capability is 99 model measurements with the first position of each pressure switching valve being used for transducer calibration

Each channel includes two pressure measuring transducers (referenced to hard vacuum). The two measuring transducers, a ±1-psid unit and a 0- to 15-psid unit, are switched in and out of the system automatically to allow measuring to the best available precision. If the sensed pressure level is above 15 psia, the reference side of the 15-psid transducer is vented to atmosphere to extend the measuring range.

The measuring system is of the Wiancko frequency modulation type. Precision frequency modulation oscillators, frequency multipliers, binary counters, and a time base generator operate in conjunction with the transducers to obtain a differential count of 10, 000. The resulting resolution is 0. 0002 psi for the 1-psi transducer and 0. 0015 psi for the 15-psid transducers. The accumulated count is stored in the binary counters, read out serially by the ERA scanner, and punched on paper tape.

The p_o system contains two channels of frequency modulation pressure instrumentation, one with a range of 0 to 500 psia and the other with a range of 0 to 2500 psia.

2.3.2 Pressure Distribution Phase, 50-Inch Mach 8 Tunnel (B)

The model pressures were measured with nine Wiancko pressure transducers, rated at 5 psid, connected selectively to seven independently variable reference pressures which were constantly monitored by seven CEC Electromonometers, rated at 1, 5, 15, and 30 psia.

This system will automatically select the proper instrument sensitivity and absolute reference pressure to ensure measurement of the model pressures to the best available precision. Three instrument sensitivities, calibrated to obtain full-scale deflection for ±0. 3, ±0. 6, and ±1. 2 psid, were used in conjunction with the seven reference pressures, which varied in approximately 2-psia increments from nearly zero pressure.

The pressure side of each Wiancko transducer was inserted into the outlet of a Giannini 12-position rotary valve. Reference pressure was connected to the first valve inlet position to obtain the instrument zero. Various model pressure taps were connected in the desired order to the required number of the remaining eleven valve inlets. The transducer outputs were measured with Leeds and Northrup self-balancing, millivolt potentiometers equipped with Coleman digital read-out units. The potentiometer readings were punched on paper tapes by a high-speed punch.

The tunnel stagnation pressure and temperature were measured in the stilling chamber. A 1000-psid transducer, referenced to vacuum, and a chromel-alumel thermocouple were used for the measurement.

2.3.3 Heat-Transfer Phase

The reference junction of each thermocouple was maintained at 132°F. Each thermocouple output was recorded in digital form on magnetic tape at a rate of 20 times per second by means of a Beckman 210 analog-to-digital converter. To monitor the temperatures at selected points on the models, nine of the thermocouple outputs were also recorded on strip charts by 0.25-sec (full-scale travel) Brown servo-potentiometers.

3.0 TEST DESCRIPTION

3.1 TEST PROCEDURE

The exit configurations were tested at a nominal Mach number of 8 except for the modified exit heat-transfer model which was tested at a nominal Mach number of 10. The re-entry configurations and the hemisphere-cylinder models were tested at a nominal Mach number of 10. Tunnel conditions and model attitudes at which data were obtained are summarized in Table 1.

Selected pressure taps were visually monitored during the pressure phase to determine when the model pressures reached equilibrium, after which the data were recorded.

The transient heat-transfer testing on the exit configuration in the 50-Inch Mach 8 Tunnel (B) utilized cooling shoes to cool the model. Between data runs, the model was enclosed in cooling shoes into which cold air was introduced to cool the model to approximately 32°F. These shoes (split in the vertical plane) were retracted to the tunnel walls before recording the heat-transfer data. The hydraulically actuated cooling shoe

mechanisms were mounted in place of the windows. A photograph of the interior of the test section of the tunnel showing the original exit heat-transfer model with the shoes retracted to the tunnel sidewalls is presented in Fig. 6a. Because of the large base diameter of the exit models, the shock wave from the retracted cooling shoes impinged upon the aft section of the model. Rather than test the modified exit model under these conditions, the heat-transfer phase of the test was performed in the 50-Inch Mach 10 Tunnel (C).

Transient heat-transfer testing in the 50-Inch Mach 10 Tunnel (C) was accomplished by utilizing the tunnel injection system. With the model lowered into the installation chamber, ambient air is ducted into the tank through strategically located ports which are baffled to allow the cooling air to be directed toward the model. Upon reaching a desired model temperature, the model was injected into the tunnel, and the temperature-time data were recorded.

Shadowgraphs were obtained using a conventional, short-range, divergent-ray, spark shadowgraph system. Selected model attitudes at both the high and low Reynolds number for all configuraions were recorded by this shadowgraph system.

3.2 DATA REDUCTION PROCEDURE

Each pressure was measured and recorded, and the raw data were reduced to pressure values by the VKF ERA 1102 digital computer. Besides computing the pressure, the computer also calculated the value of the coefficient of pressure (C_p), ratio of local pressure to tunnel stagnation pressure (p/p_o), and the ratio of local pressure to the pressure behind a normal shock (p/p_{t_2}). The values of p_∞, p_{t_2}, and q were calculated from isentropic equations utilizing the measured tunnel stagnation pressure and a Mach number based on an average test section Mach number obtained from tunnel calibration. The perfect gas equation of state was used to calculate tunnel parameters in the 50-Inch Mach 8 Tunnel (B); however, the Beattie-Bridgeman equation of state assuming variable specific heats as presented in Ref. 2 was used to calculate tunnel parameters in the 50-Inch Mach 10 Tunnel (C).

The heat-transfer rate was calculated from the standard equation

$$q = wbc\ dT/dt$$

The heat-transfer coefficient was then calculated from

$$h = q/(T_o - T_w)$$

The values of T_W and dT/dt were calculated by a second degree equation obtained by using the method of least-squared through 21 consecutive points of the temperature-time data. The values of skin thickness used in determining the heating rates are listed in Tables 2, 3, and 4. The values of the thermal properties of types 310 and 321 stainless steel used in the calculations are presented in Fig. 7.

4.0 RESULTS AND DISCUSSION

Representative results of the tests performed on the Gemini configuration are presented in Figs. 8 to 12 and 14 to 16. Basic pressure and heat-transfer distribution data are presented for the exit configurations and the re-entry configuration in Figs. 10, 12, and 16. The pressure and heat-transfer distributions on the heat shield of the re-entry configuration are of particular interest and are presented in Figs. 14 and 15. The pressure and heat-transfer distribution on the hemisphere-cylinder at $M_\infty = 10$ are presented in Fig. 13. In all cases, the heat-transfer data are presented as a ratio of measured heat-transfer coefficient to the theoretical value of the heat-transfer coefficient at the stagnation point of the model at zero-deg angle of attack. In a similar manner, the pressure data are presented as the ratio of measured model pressure to the pressure behind a normal shock.

Since the heat-transfer data are presented as a ratio of a theoretical value, a comparison of the measured heat-transfer rates at the stagnation point when the model is at a pitch angle of zero deg with theory is necessary. This comparison is presented as a function of Nusselt number and Reynolds number in Fig. 8. The criteria for using these parameters is that the stagnation point theory for all spherical-shaped noses lie on one curve. The stagnation point theory used in presenting these data is that of Fay and Riddell (Ref. 3). The theoretical value of the rate of heat transfer was calculated as suggested in Ref. 3 (assuming Lewis number as unity) and then transformed into a Nusselt number. The values of velocity gradient used in calculating the Fay and Riddell theory and the correlation Reynolds number were obtained from the work of Boison and Curtiss, documented in Ref. 4. The density and viscosity terms in the Reynolds number equation were evaluated at a bulk temperature as was the thermal conductivity term in the Nusselt number. Bulk temperature is defined as an average between the model wall temperature and the tunnel stagnation temperature. The measured heat-transfer data were transformed by the above method.

The fact that the stagnation point data is approximately 30 percent higher than theory at the maximum Reynolds number and 15 percent higher

than theory at the minimum Reynolds number on the re-entry configuration cannot be explained at this time. Additional work is being instigated in an attempt to explain these discrepancies. It is interesting to note, however, the excellent comparison between theoretical and experimental results obtained on the modified exit configuration and the hemisphere-cylinder configuration.

The pressure and heat-transfer distribution on the original and modified exit configurations are compared in Fig. 9. The value of h_{S_t} used in the calculation of h/h_{S_t} for both configurations was based on the flat nose of the modified configuration of Mach numbers of 8 and 10. This approach was assumed because a theoretical stagnation point heat-transfer coefficient for the original configuration could not be calculated confidently because of the lack of a well-defined stagnation point velocity gradient.

Sketches of the shock shapes about the exit configurations recorded by the shadowgraph system are presented in Fig. 10. Because of the size of the model, only a portion of the shock waves was recorded. Consequently, the top portion of the model is presented at α = 0 deg and the bottom portion at α = 10 and 20 deg. A comparison of the shock shapes at α = 0 deg shows the bow shock on the original configuration to be much closer to the body than the bow shock of the modified configuration. At α = 10 deg, over the bottom of the model, the opposite is evident. The effect of the intersection of the bow shock with the shock emanating from the collar-body junction is more pronounced on the modified exit configuration.

A comparison of the flow over the exit model with and without the horizon scanner is presented in Figs. 11 and 12. The data for the configuration with no horizon scanner were obtained from the bottom ray (Φ = 180-deg ray) at α = 20 deg. Data were also obtained at α = 20 deg (Φ = 90-deg ray) to determine the effect of the horizon scanner in the windward position. The most interesting occurrence was the increase in heat-transfer rates at the reattachment point of the flow just aft of the horizon scanner. Downstream of the latches on the adapters, the effect of the horizon scanner was insignificant.

The pressure and heat-transfer distributions on the hemisphere-cylinder configuration are presented in Fig. 13 for zero-deg angle of attack. This figure indicates that the heat-transfer distribution was essentially uniform over the top and bottom hemispherical surfaces and that the stagnation point heating rate was less than five percent higher than the theoretical value. The pressure distribution over the hemisphere was symmetrical and agreed well with values predicted by modified Newtonian approximations.

It is evident in Fig. 14 that the heating rates obtained on the heat shield of the re-entry configuration were appreciably higher (approximately 25 to 30 percent) than the theoretical stagnation point heating rate. The lack of symmetry in the heat-transfer data at zero angle of attack is attributed to small disturbances in the flow near the axis of the tunnel inasmuch as the distributions remained fixed with respect to the tunnel when the model was rolled. The effect of these disturbances appears to vary with the location of the model in the tunnel because the first day's testing was conducted with the nose of the model about 1.75 in. upstream of the center of upstream window, and the second day's testing was with the nose about 1.50 in. further upstream. The size and bluntness of the Gemini configuration may have contributed to the sensitivity of this model to the disturbances since the hemisphere-cylinder heat-transfer distribution was much more symmetrical. Both of the hemisphere-cylinder models (heat-transfer and pressure distribution) and Gemini re-entry pressure distribution model were located with the noses of the models about seven inches downstream of the center of the upstream window.

As shown in Figs. 14 and 15, the influence of the tunnel flow disturbances decreased as the angle of attack increased, and the general trend of the data on the heat shield appears to be reasonable. The rapid increase in heat-transfer rates between the stagnation point and the edge of the heat shield on the windward side is indicative of the increasing velocity gradients in this region.

The heat-transfer and pressure distribution over the body, collar, and antenna housing of the re-entry model are presented in Fig. 16. The negative angles of attack are presented for the windward ray (Φ = 180-deg ray) and leeward ray (Φ = 0-deg ray) to show the general pressure and heat-transfer distribution on this type of model geometry. The fact that the pressures are slightly higher on the top ray is probably an indication of the relative strength of the separation region. Since the flow does not reattach until the aft portion of the collar, the pressure level in the separated region is a strong function of the velocity and pressure gradients on the heat shield.

The attachment point is quite evident at higher angles of attack. The heat-transfer data indicate that the attachment point occurs nearer the heat shield than indicated by the pressure data. The difference between these points could depend on a number of reasons. The following are some of the possibilities: differences in model wall temperature, stability of the geometry of the heat-transfer model during the heating cycle, and also the location of the sonic point and separation point at the edge of the heat shield.

5.0 CONCLUDING REMARKS

Generally, the pressure and heat-transfer distribution on both the exit and re-entry configurations occurred as expected. At zero-deg angle of attack, the flow was completely separated over the body of the re-entry configuration with reattachment on the collar. Not until angles of attack greater than 30 deg did the heat-transfer rates on the collar become excessive on the re-entry configuration. At α = 40 deg, a heating rate of approximately 3.2 times larger than stagnation point theory was attained on the collar.

The data obtained on the exit configuration appears to be satisfactory. By modifying the exit configuration, the flow field becomes more symmetrical, and more uniform heating rates result around the model.

REFERENCES

1. Test Facilities Handbook, (4th Edition). "von Kármán Gas Dynamics Facility, Vol. 4." Arnold Engineering Development Center, July 1962.

2. Randall, R. E. "Thermodynamic Properties of Gases: Equations Derived from the Beattie-Bridgeman Equation of State Assuming Variable Specific Heats." AEDC-TR-57-10, August 1957.

3. Fay, J. A. and Riddell, F. R. "Theory of Stagnation Point Heat Transfer Measurements in Dissociated Air." Journal of Aeronautical Sciences, Vol. 25, No. 2, February 1958, pp. 73-85.

4. Boison, J. Christopher, and Curtiss, Howard A. "An Experimental Investigation of Blunt Body Stagnation Point Velocity Gradient." ARS Journal, Vol. 29, No. 2, February 1959, pp. 130-135.

TABLE 1

SUMMARY OF TEST CONDITIONS

Configuration	Model	Mach No.	Re/ft	$\alpha(\psi = 0)$, deg	$\psi(\alpha = 0)$, deg
Exit	Original Pressure and Heat Transfer	8	0.63×10^6 and 1.35×10^6	0, ±5, ±10, ±15, and ±20	0, 5, 10, 15, and 20
Exit	Modified Pressure	8	0.63×10^6 and 1.35×10^6	0, 5, 10, 15, and 20	0, 5, 10, 15, and 20
Exit	Modified Heat Transfer	10	0.63×10^6 and 1.35×10^6	0, 5, 10, 15, and 20	0, 5, 10, 15, and 20
Re-Entry	Pressure and Heat Transfer	10	0.72×10^6, 1.44×10^6, and 2.12×10^6	0, ±5, ±10, ±15, ±20, ±25, ±30*, ±35*, and ±40*	0
Hemisphere Cylinder	Pressure and Heat Transfer	10	1.0, 1.6, 2.0 and 2.4×10^6	0	0

*NOTE: Pressure data were not obtained at α = +30, +35, and +40 deg.

TABLE 2

EXIT MODEL INSTRUMENTATION

a. Nose, Original Configuration

Φ, deg \ R	0	.590	1.180
0	.0237 X	.0236 X	.0236 X
45		.0236 X	.0236 X
90		.0236 X	.0236 X
135		.0237 X	.0236 X
180		.0236 X	.0237 X

b. Nose, Modified Configuration

Φ, deg \ R	0	.590	1.180
0	.0270 X	.0270 X	.0267 X
45		.0271 X	.0267 X
90		.0271 X	.0269 X
135		.0271 X	.0268 X
180		.0270 X	.0266 X

All dimensions in inches unles otherwise noted.
Numbers denote skin thicknesses at respective T.C. locations.
X's denote pressure taps.

TABLE 2 (Continued)

c. Body, Original Configuration

Z \ Φ	0	39	74	90	135	142	180
2.344	.0236 X			.0236 X	.0235		.0236 X
2.720					X		
4.744	.0236 X		.0236 X	.0236 X	.0237 X		.0237 X
7.144	.0206 X		.0206 X	.0208 X	.0206 X		.0208 X
8.344			.0233 X		.0235 X		
8.790	.0236			.0237			.0236
9.236	.0235 X						.0235 X
9.544				.0235 X			
10.944	.0227 X	.0227 X		.0229 X			.0230 X
11.644	.0231 X	.0233 X		.0234 X	.0235 X	.0235 X	.0234 X
12.344	.0231 X	.0232 X			.0234 X	.0234 X	.0234 X
13.344	.0232 X	.0232 X		.0233 X	.0234 X		.0235 X
13.930		.0226 X					
14.344	.0231 X	.0224 X			.0234 X		.0234 X
15.344	.0232 X	.0234 X		.0230 X	.0233 X		.0234 X
16.344	.0227 X	.0234 X		.0227 X	.0233 X		.0229 X
17.128	.0235 X	.0234 X		.0235 X	.0235 X		.0238 X
17.897	.0239 X	.0234 X		.0241 X	.0236 X		.0236 X
18.897	.0233 X			.0234 X			.0233 X
19.897	.0235 X	.0235 X		.0234 X	.0235 X		.0235 X
20.347	.0234 X	.0234 X		.0235 X	.0235 X		.0233
20.947							.0235 X
21.697	.0236 X	.0236 X		.0237 X	.0237 X		.0237 X
23.197	.0236 X	.0236 X		.0237 X	.0236 X		.0236 X
23.900	.0236 X						

All dimensions in inches unless otherwise noted.
Numbers denote skin thicknesses at respective T.C. locations.
X's denote pressure taps.

TABLE 2 (Concluded)

d. Body, Modified Configuration

Z \ Φ	0	39	60	62	65	70	74	80	90	135	142	180
2.040										.0235		
2.344	.0236 X								.0236 X			.0236 X
2.720										X		
4.744	.0236 X						.0236 X		.0236 X	.0237 X		.0237 X
5.775									.0240			.0239
6.275	.0236								.0240	.0239		.0237
6.475									.0239			.0237
7.144	.0206 X						.0206 X		.0208 X	.0206 X		.0208 X
8.344							.0233 X			X		
8.990	.0236								.0237			
9.040												.0236
9.236	.0235 X											.0235 X
9.544									.0235 X			
10.944	.0227 X	.0227 X							.0229 X			.0230 X
11.644	.0231 X	X							X	X	X	X
12.344	X	.0232 X								.0234 X	X	.0234 X
13.344	.0236 X	.0212 X							.0238 X	.0239 X		.0239 X
13.930		.0233 X										
14.344	.0236 X	.0224 X							.0239	.0237 X		.0239 X
14.844				.0234		.0227		.0236	.0235			
15.344	.0235 X	.0234 X				.0235			.0232 X	.0237 X		X
15.844				.0224		.0225		.0233	.0230			
16.344	.0234 X	.0234 X	X	.0234				.0250	.0243	.0234 X		.0237 X
17.128	.0234 X	.0234 X	.0235 X					.0239	.0239	.0234 X		.0236 X
17.897	.0239 X	.0237 X	.0241 X					.0250	.0250	.0206 X		.0244 X
18.350					.0235			.0251				
18.897	.0239 X					.0237		.0250	.0249	X		.0239 X
19.500						.0238		.0235				
19.897	.0239 X	.0236 X							.0236 X	.0226 X		.0239 X
20.347	.0242 X	.0233 X							.0234 X	.0236 X		.0250
20.947												X
21.697	.0249 X	X							.0247 X	.0247 X		.0250 X
23.197	.0244 X	.0246 X							.0248 X	.0251 X		.0249 X

All dimensions in inches unless otherwise noted.
Numbers denote skin thicknesses at respective T. C. locations.
X's denote pressure taps.

TABLE 3

RE-ENTRY MODEL INSTRUMENTATION

a. Heat Shield

R / Φ, deg	0	.252	.499	.999	1.497	2.001	2.505	2.995	3.513	3.900	4.003	4.200	4.348	4.400
0	.0271 X	.0273		.0274 X	.0273	.0272 X	0.273	.0274 X	.0274		.0275 X			
45				.0271 X		.0273 X		.0273 X			.0272 X			
66.5												.0273		.0273
69.5										.0272		.0273		.0273
74.5										.0272		.0275		.0275
79.5										.0273		.0276		.0276
83.5												.0276		.0276
90				.0270 X		.0270 X		.0272 X			.0272 X			
96												.0274		.0274
99										.0277		.0274		.0274
104.5										.0277		.0275		.0275
109										.0276		.0276		.0277
112.5												.0277		.0277
135				.0270 X		.0271 X		.0272 X			.0275 X			
157.5				.0271 X		.0271 X		.0273 X			.0275 X		X	
180			.0272 X	.0272 X	.0272 X	.0272 X	.0272 X	.0274 X	.0275 X		.0276 X		.0276 X	
276.5												.0269		.0269
280.5										.0273		.0269		.0269
284.5										.0273		.0270		.0270
290.5										.0273		.0271		.0271
293.5												.0271		.0271

All dimensions in inches unless otherwise noted.
Numbers denote skin thicknesses at respective T. C. locations.
X's denote pressure taps.

TABLE 3 (Concluded)

b. Body

Z \ Φ	0	39	63	68	73	78	82	90	123	135	142	180	218	225	228	232	237
10.344														.0290	.0290		
10.500					.0280	.0280											
10.644			.0280	.0280		.0280	.0260		.0283				.0272		.0290	.0266	.0278
10.944	.0282 X	.0280 X						.0282 X				.0282 X					
11.150			.0280	.0280	.0280	.0280	.0280		.0284				.0280	.0281		.0280	.0280
11.644	.0284 X	.0283 X	.0280	.0280	.0280			.0282 X	.0286	.0282 X	X	.0282 X					.0280
12.344	.0283 X	.0282 X								.0282 X	X	.0282 X					
13.344	.0286 X	.0275 X						.0284 X		.0283 X		.0283 X					
13.637		.0215															
13.930		.0240 X															
14.137		.0240															
14.344	.0286 X	.0240 X						.0284		.0283 X		.0284 X					
14.844		.0240															
15.344	.0286 X	.0240 X						.0285 X		.0284 X		.0285 X					
16.344	.0286 X	.0240 X						.0285 X		.0284 X		.0284 X					
17.128	.0280 X	.0200 X						.0285 X		.0280 X		.0273 X					
17.897	.0284 X	.0270 X						.0284 X		.0278 X		.0272 X					
18.397	.0289							.0286				.0272					
18.897	.0284 X							.0284 X				.0274 X					
19.397	.0284							.0286				.0270					
19.897	.0282 X	.0281 X						.0280 X		.0275 X		.0266 X					
20.347	.0228 X	.0233 X						.0230 X		.0233 X		.0227					
20.947	.0283							.0244				.0239 X					
21.697	.0240 X	.0238 X						.0244 X		.0243 X		.0244 X					
22.277	.0247							.0248				.0242					
23.197	.0244 X	.0245 X						.0243 X		.0245 X		.0228 X					

All dimensions in inches unless otherwise noted.
Numbers denote skin thicknesses at respective T. C. locations.
X's denote pressure taps.

TABLE 4

HEMISPHERE-CYLINDER INSTRUMENTATION

R / Φ, deg	Q	.200	.400	.600	.800	1.000	1.200	1.300	1.400	1.974	2.478	2.982	3.254	3.486	3.606
0	.0318	.0310	.0318	.0315	.0315	.0306	.0299	.0294	.0291	.0287	.0284	.0286	.0290	.0295	.0302
45			.0317		.0315		.0299	.0295	.0292						
90		.0311	.0316	.0315	.0314	.0306	.0299	.0294	.0291	.0288	.0285	.0286	.0290	.0295	.0302
135			.0318		.0314		.0298	.0295	.0293						
180		.0310	.0317	.0315	.0314	.0306	.0299	.0295	.0292	.0286	.0284	.0286	.0290	.0295	.0302
225			.0317		.0315		.0300	.0294	.0291						
270		.0311	.0318	.0315	.0314	.0306	.0300	.0296	.0291	.0287	.0285	.0286	.0290	.0295	.0301
315			.0317		.0315		.0299	.0295	.0292						

All dimensions in inches unless otherwise noted.
Numbers denote skin thicknesses at respective T.C. locations.
Pressure tap locations identical to T.C. locations.

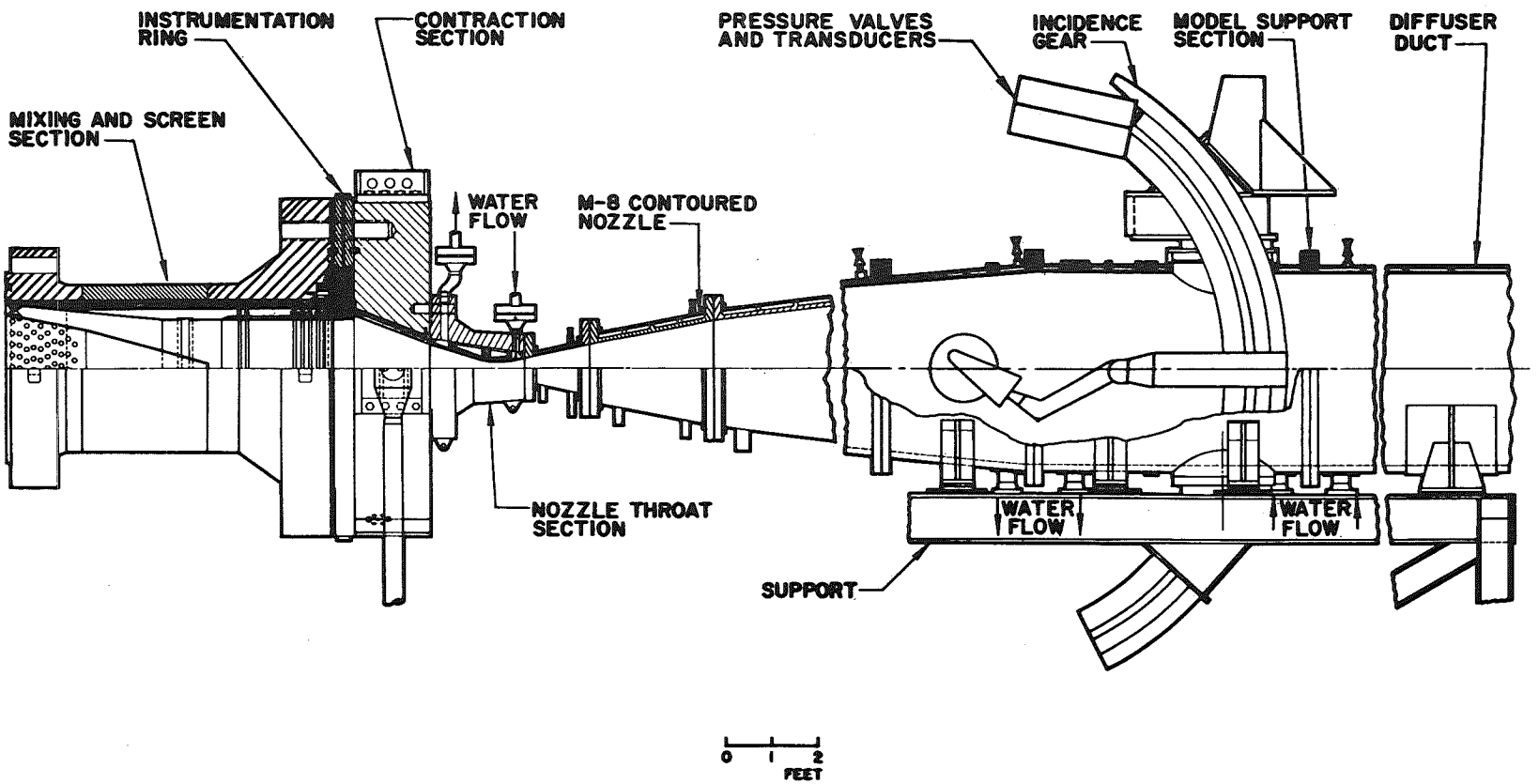

Fig. 1 The 50-Inch Mach 8 Tunnel (B)

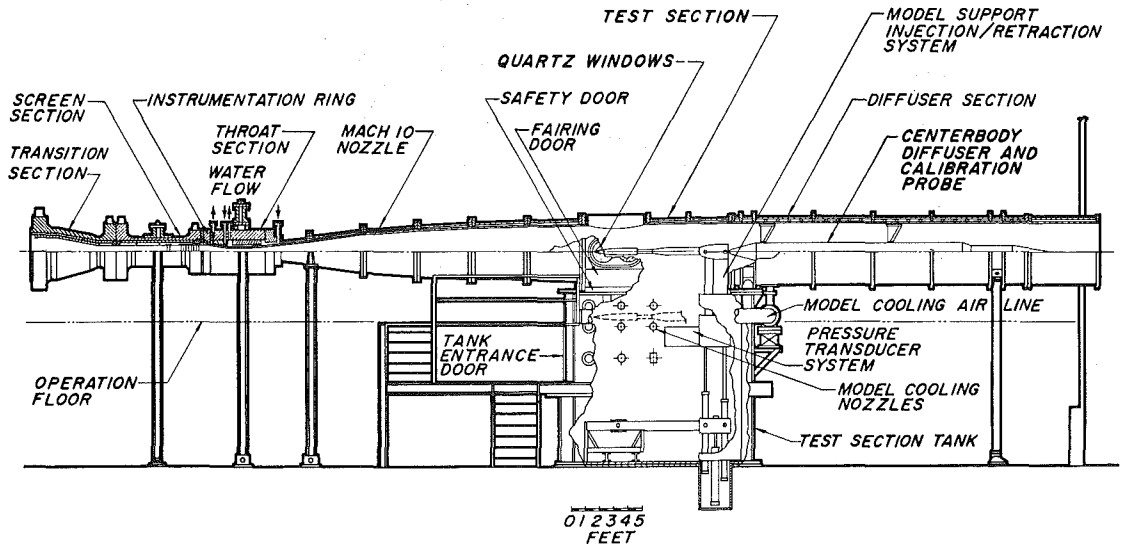

a. Tunnel Assembly

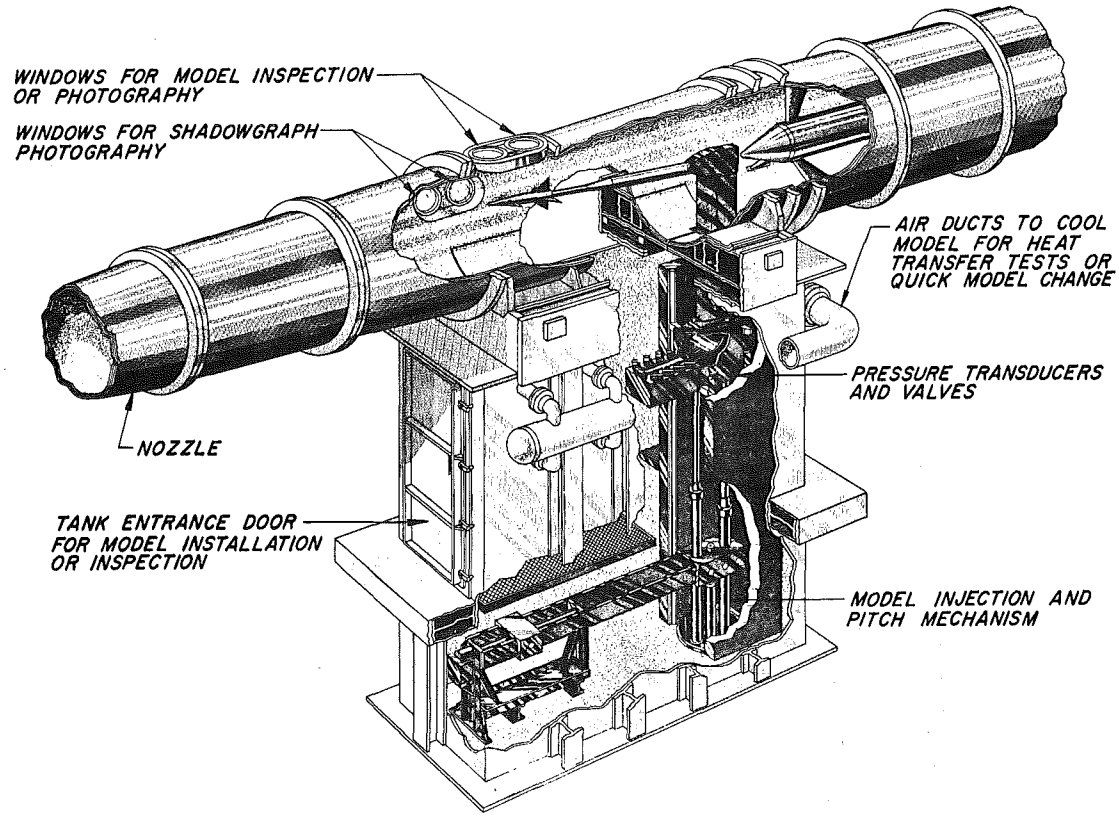

b. Tunnel Test Section

Fig. 2 The 50-Inch Mach 10 Tunnel (C)

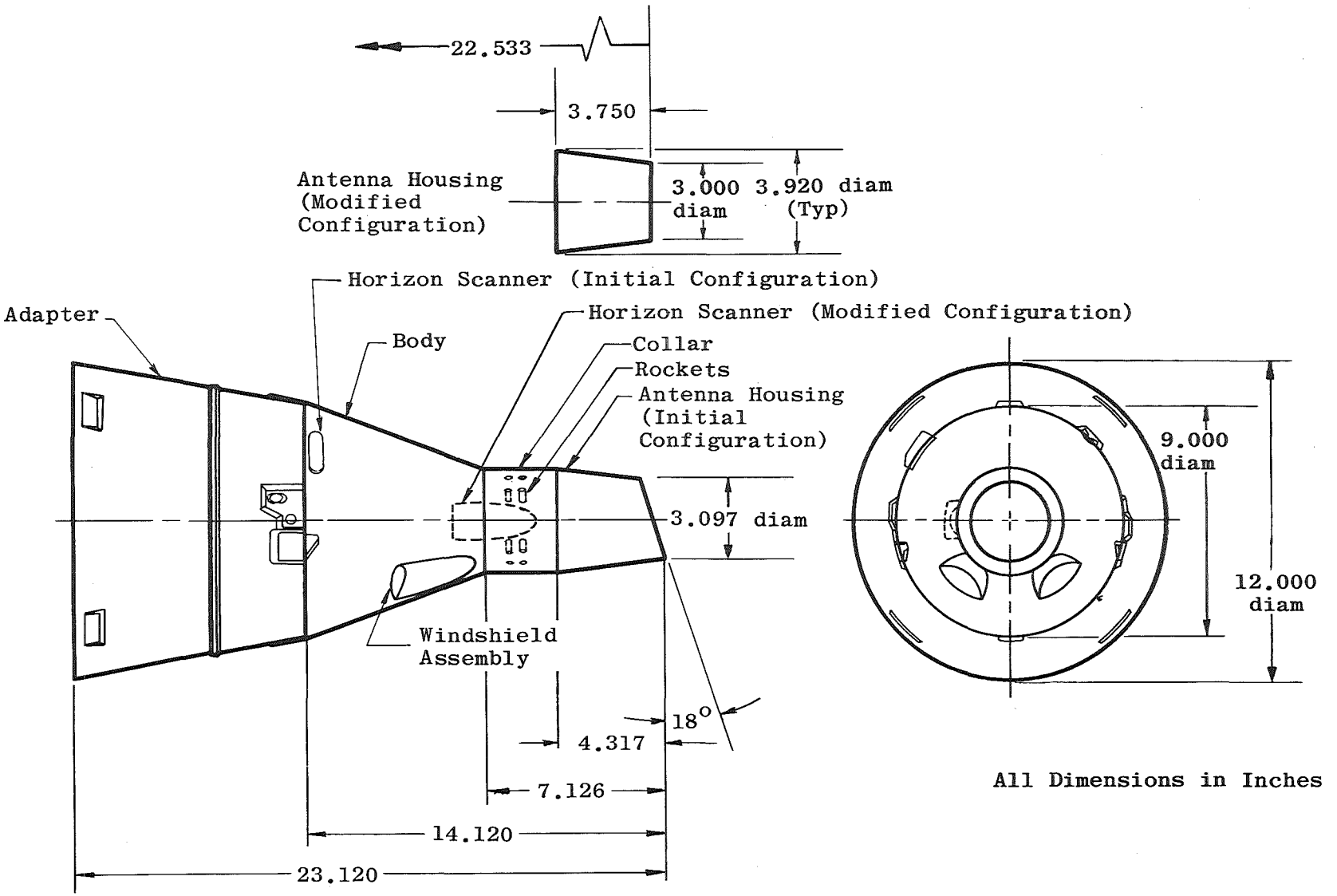

a. Model Geometry

Fig. 3 Gemini Exit Configurations

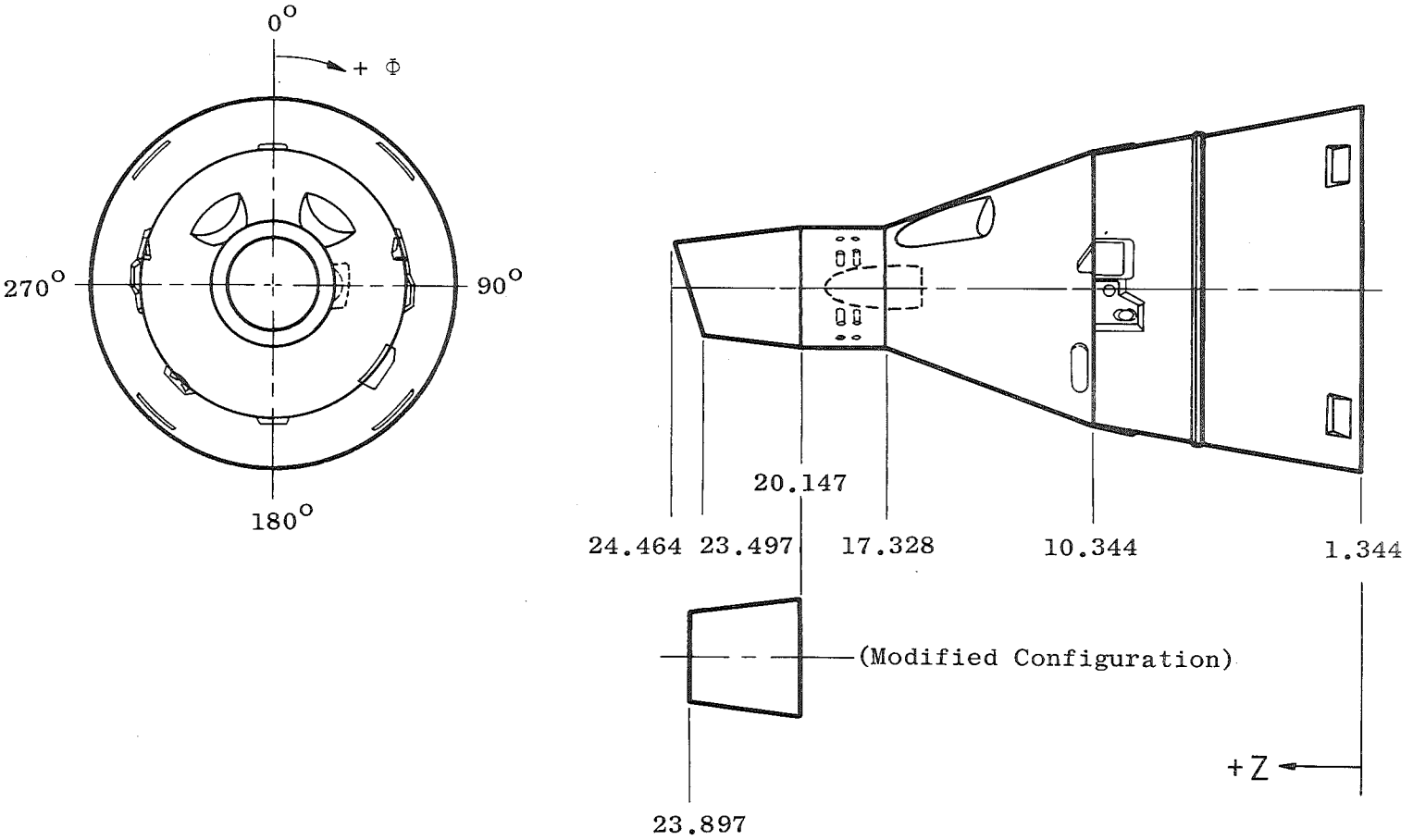

b. Notation Used for Instrumentation Locations

Fig. 3 Concluded

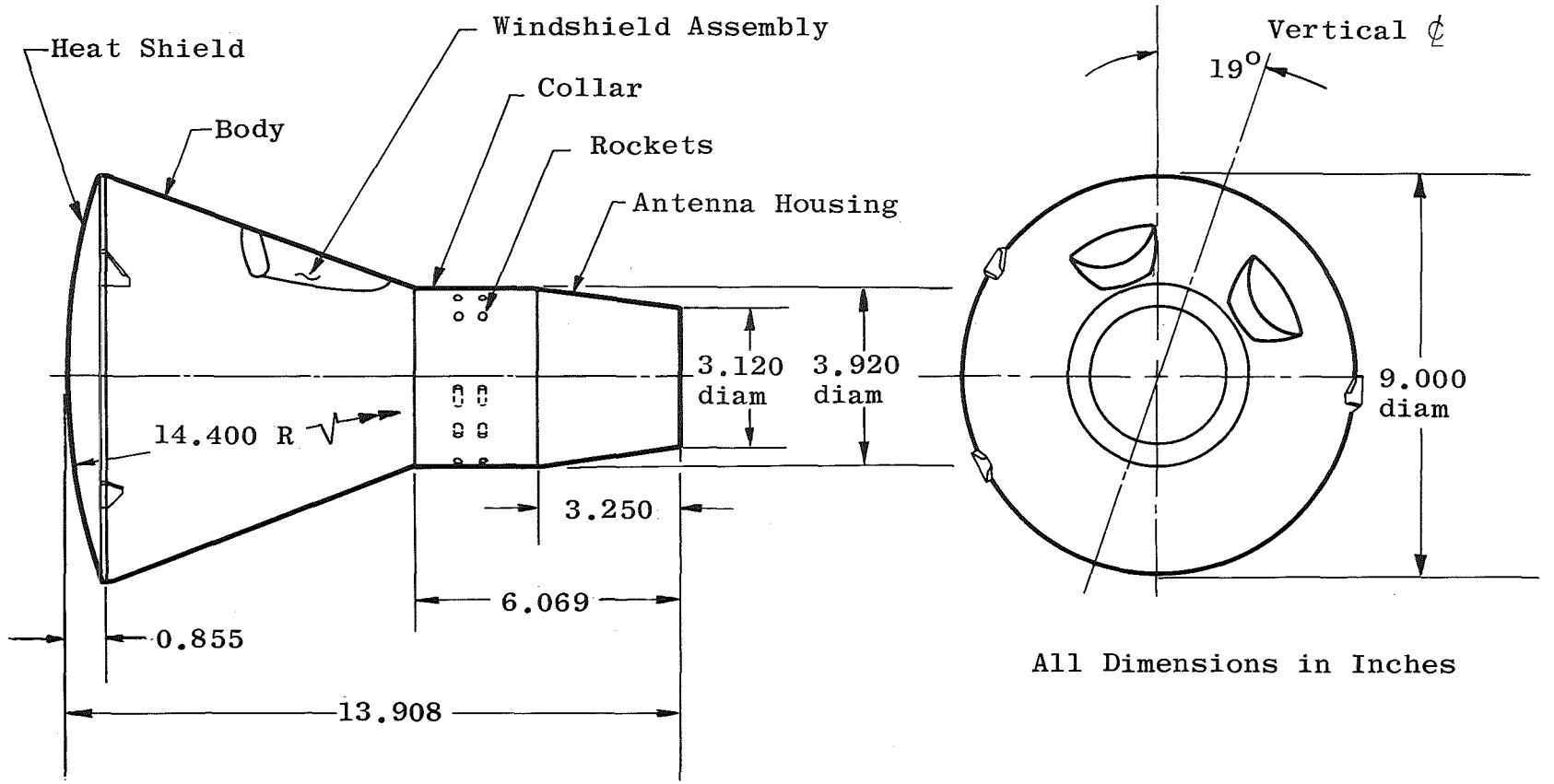

a. Model Geometry

Fig. 4 Gemini Re-Entry Configuration

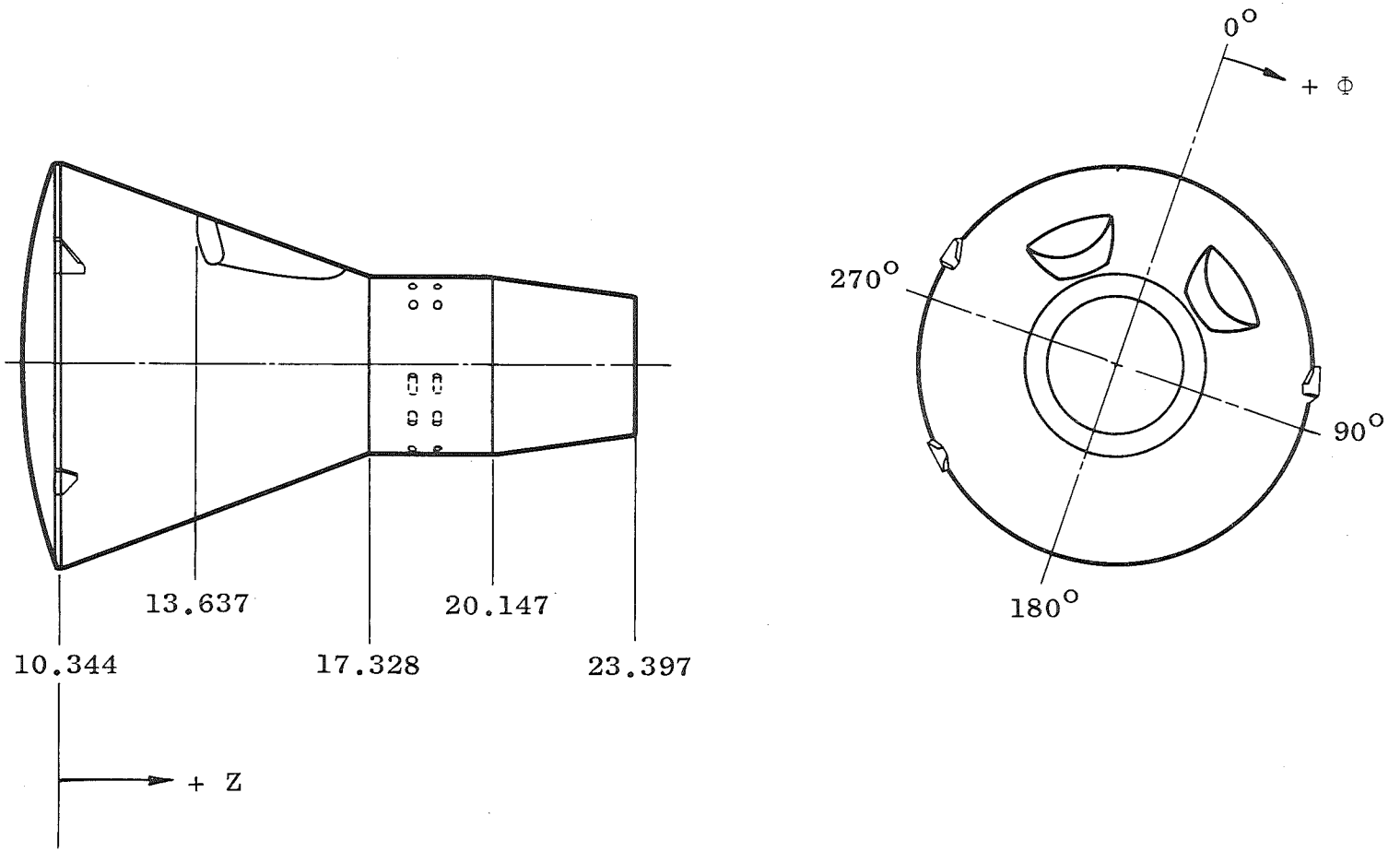

b. Notation Used for Instrumentation Locations

Fig. 4 Concluded

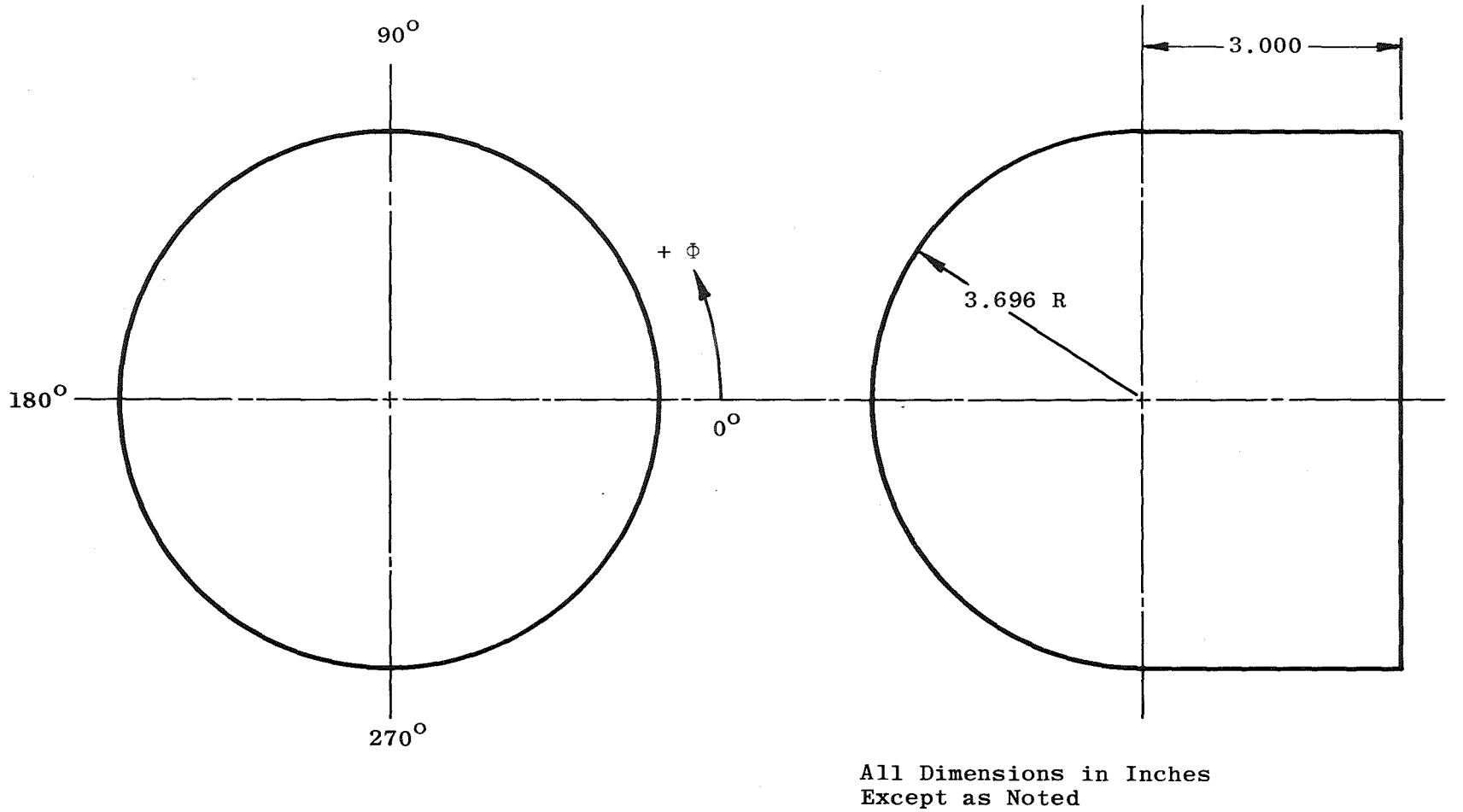

Fig. 5 Geometry of Hemisphere-Cylinder Configuration

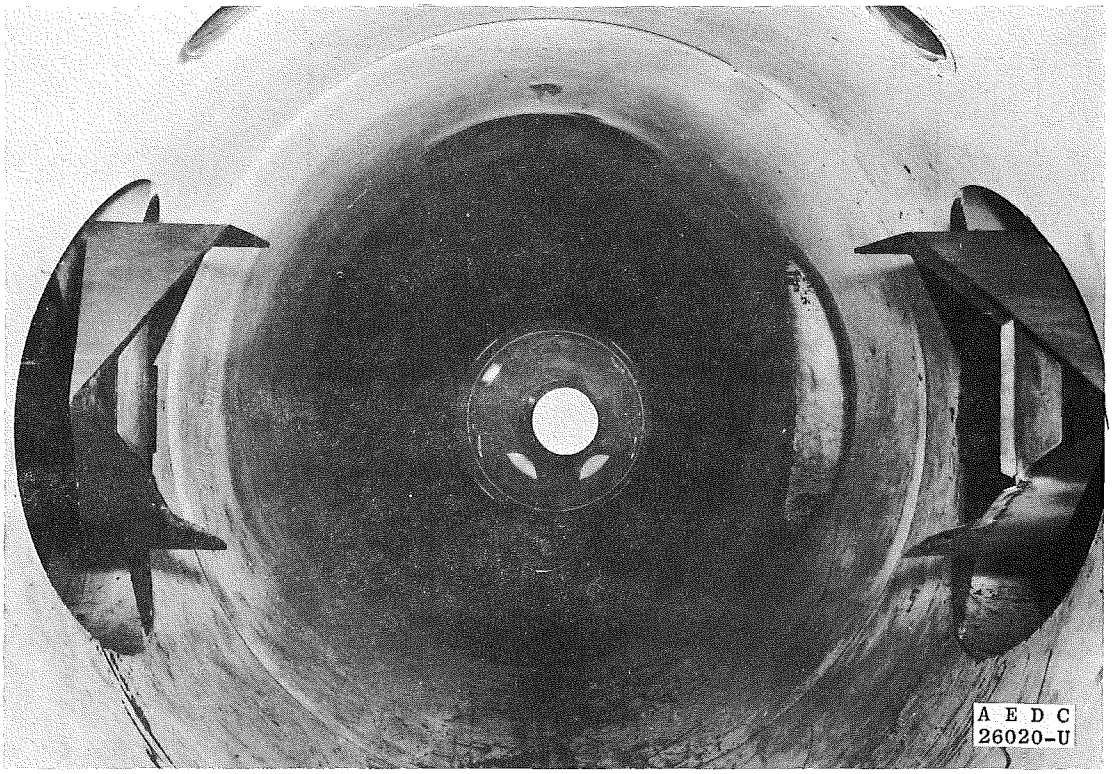

a. Original Exit Heat-Transfer Model in the 50-Inch Mach 8 Tunnel (B)

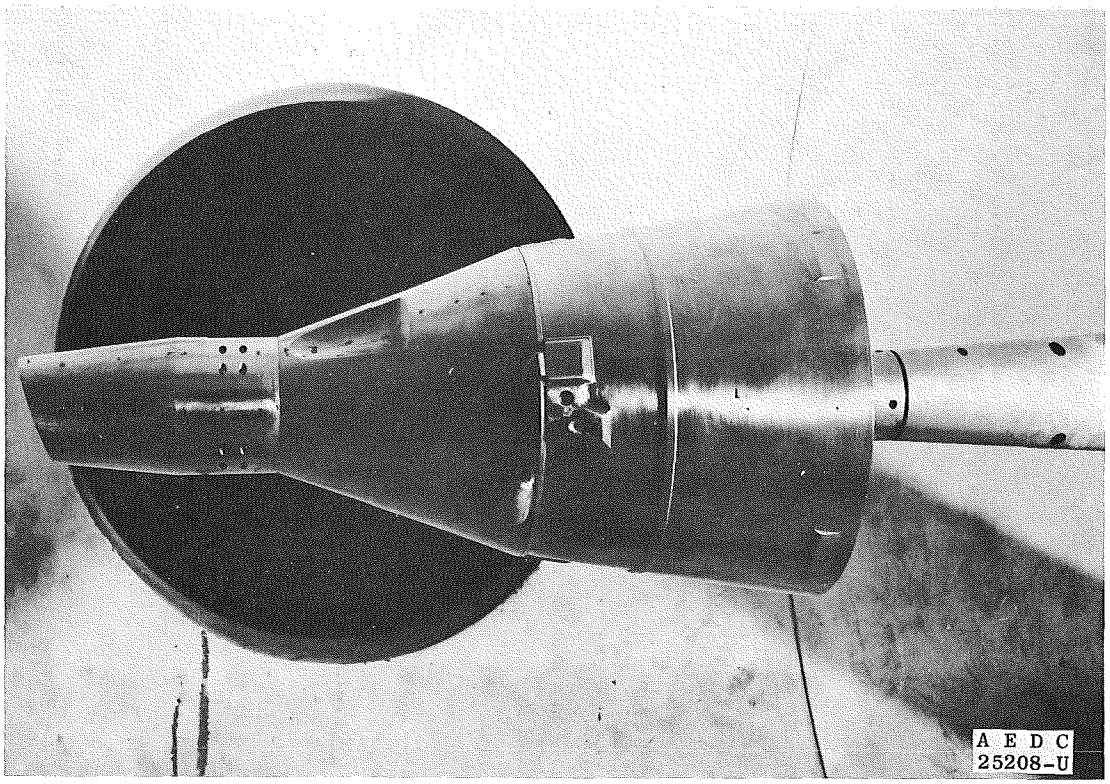

b. Original Exit Pressure Model in the 50-Inch Mach 8 Tunnel (C)

Fig. 6 Model Photographs

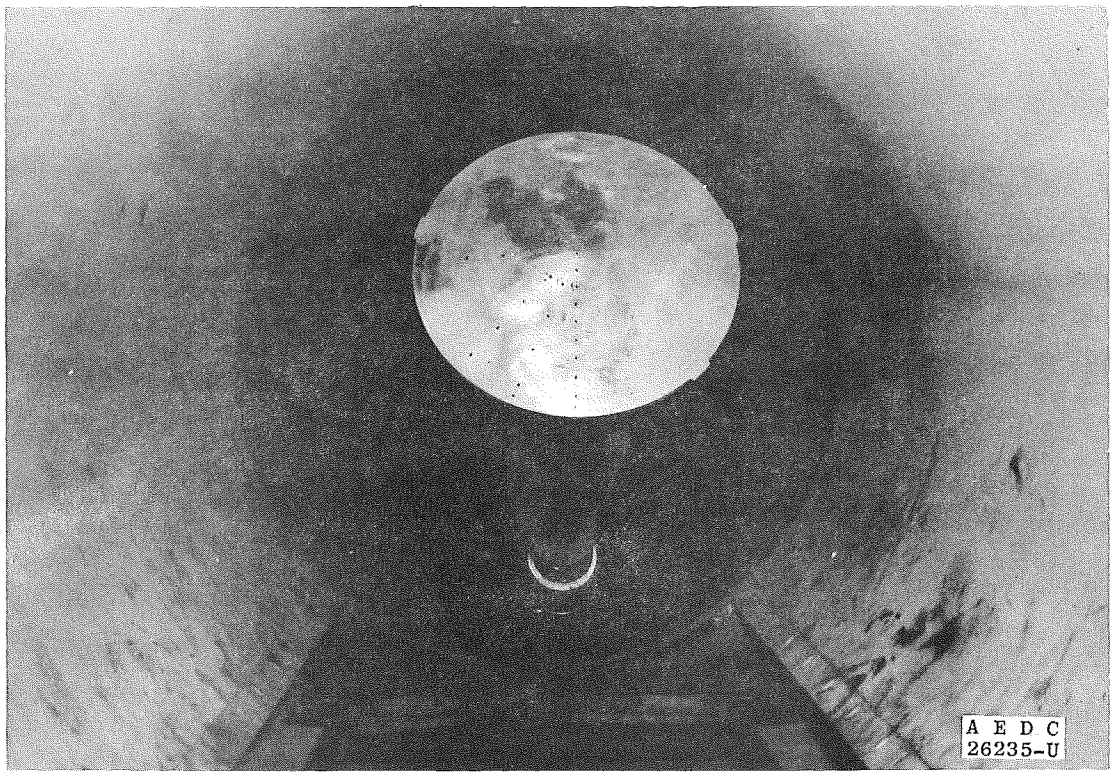

c. Front View of the Re-Entry Pressure Model in the 50-Inch Mach 10 Tunnel (C)

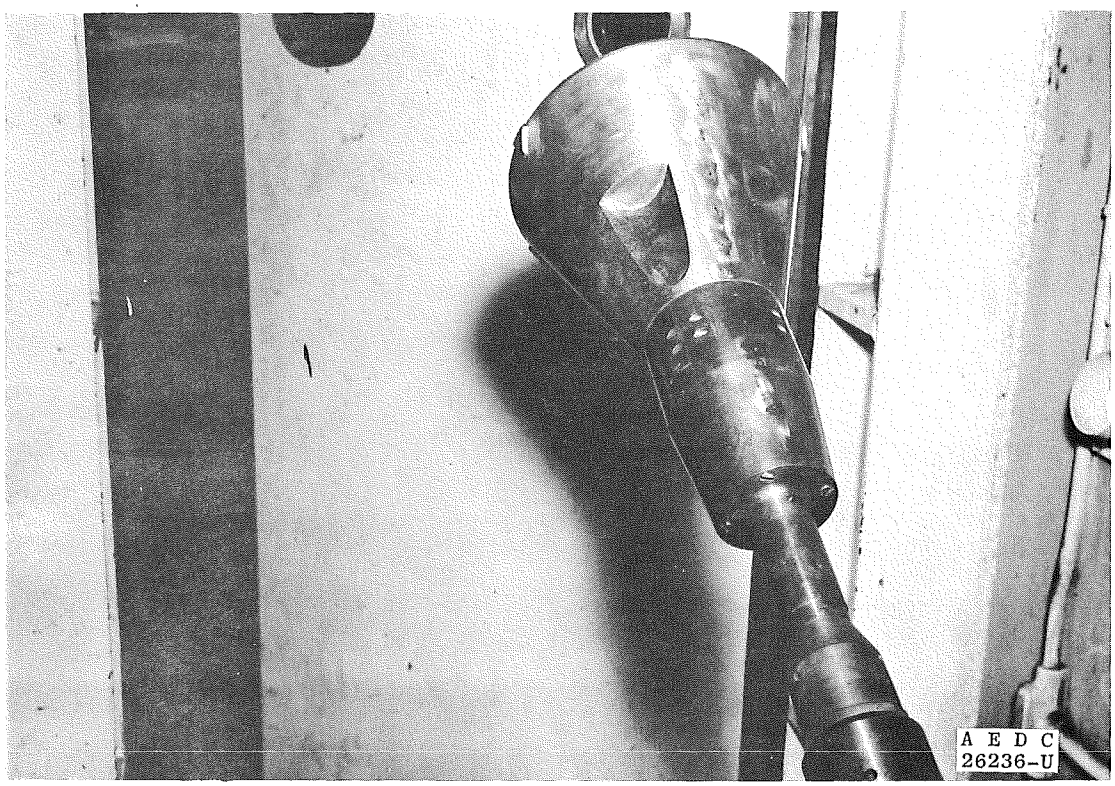

d. Rear View of the Re-Entry Pressure Model in the 50-Inch Mach 10 Tunnel (C)

Fig. 6 Continued

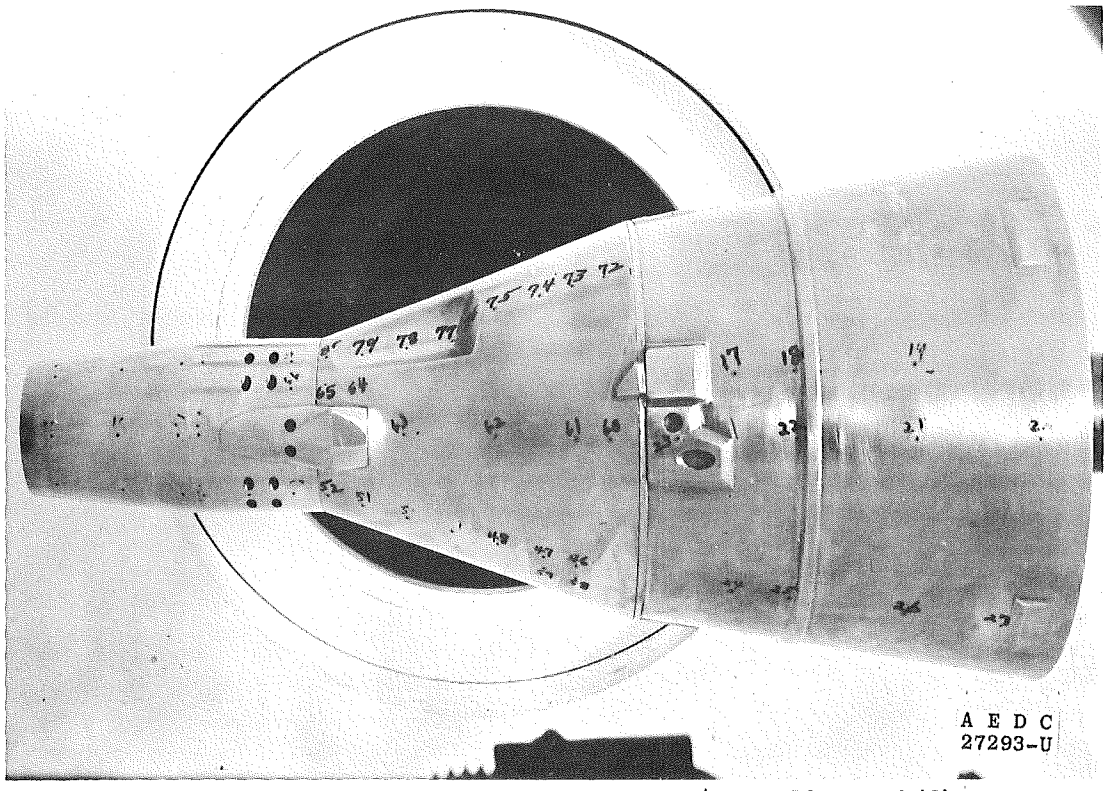

e. Modified Exit Pressure Model in the 50-Inch Mach 10 Tunnel (C)

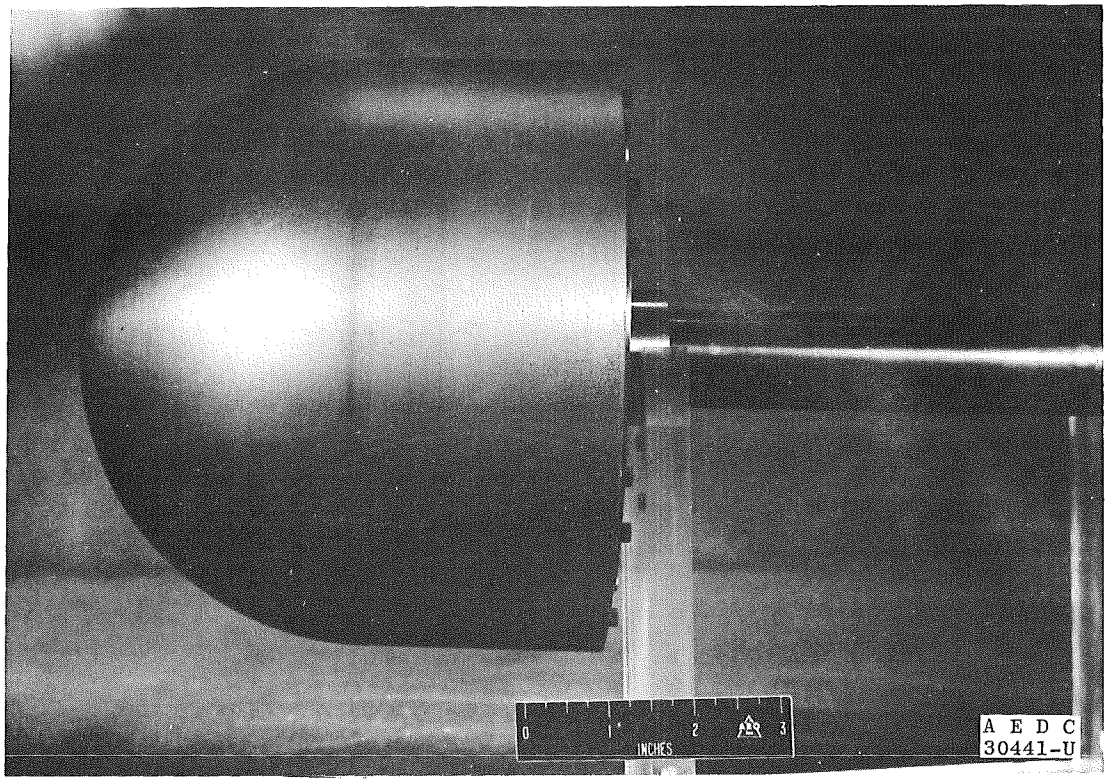

f. Hemisphere-Cylinder Heat-Transfer Model

Fig. 6 Concluded

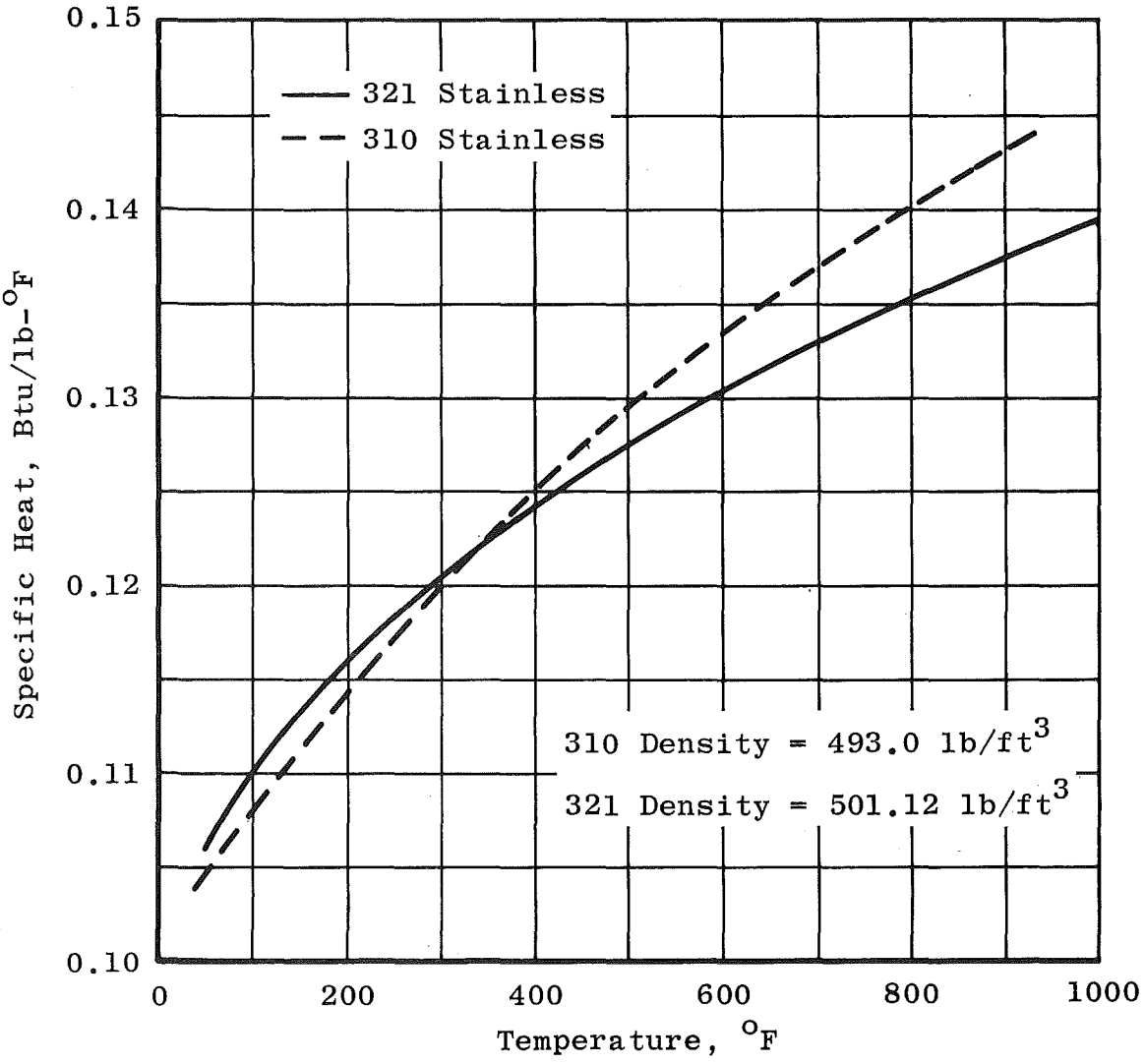

Fig. 7 Specific Heat of Types 310 and 321 Stainless Steel

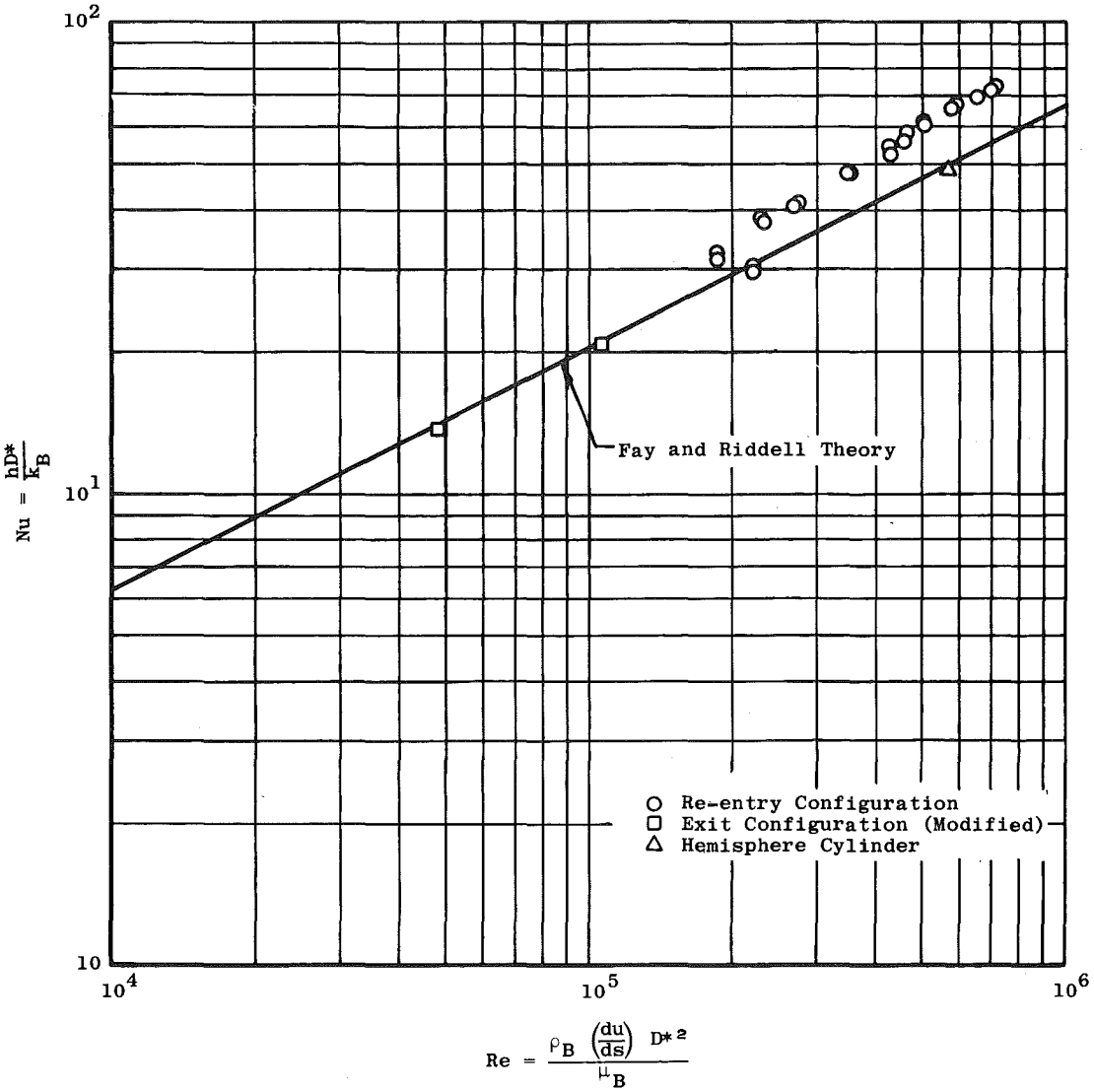

Fig. 8 Comparison of Stagnation Point Heating Rates with Theory, α = 0 deg

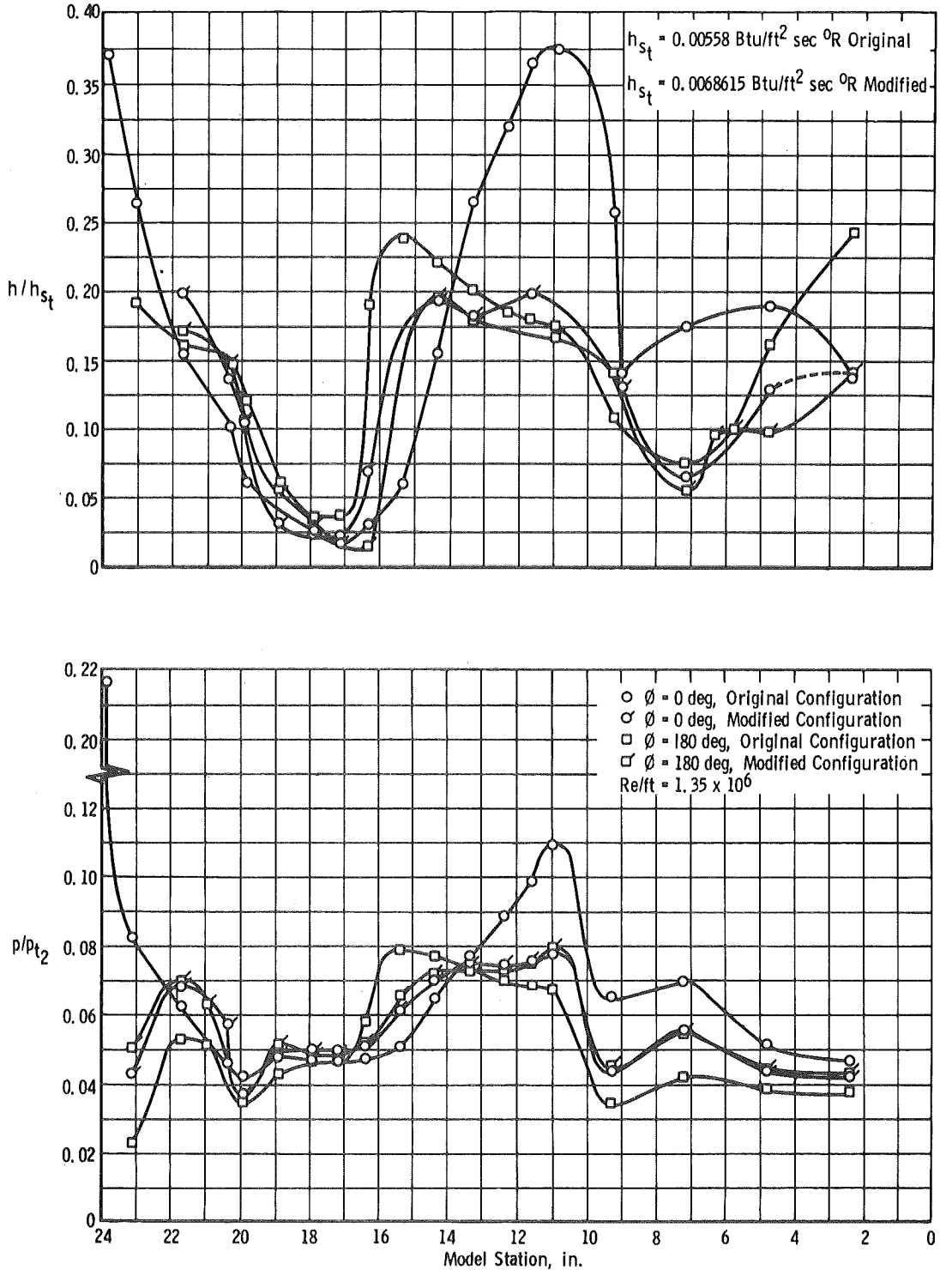

Fig. 9 Comparison of Pressure and Heat-Transfer Distributions on the Exit Configurations

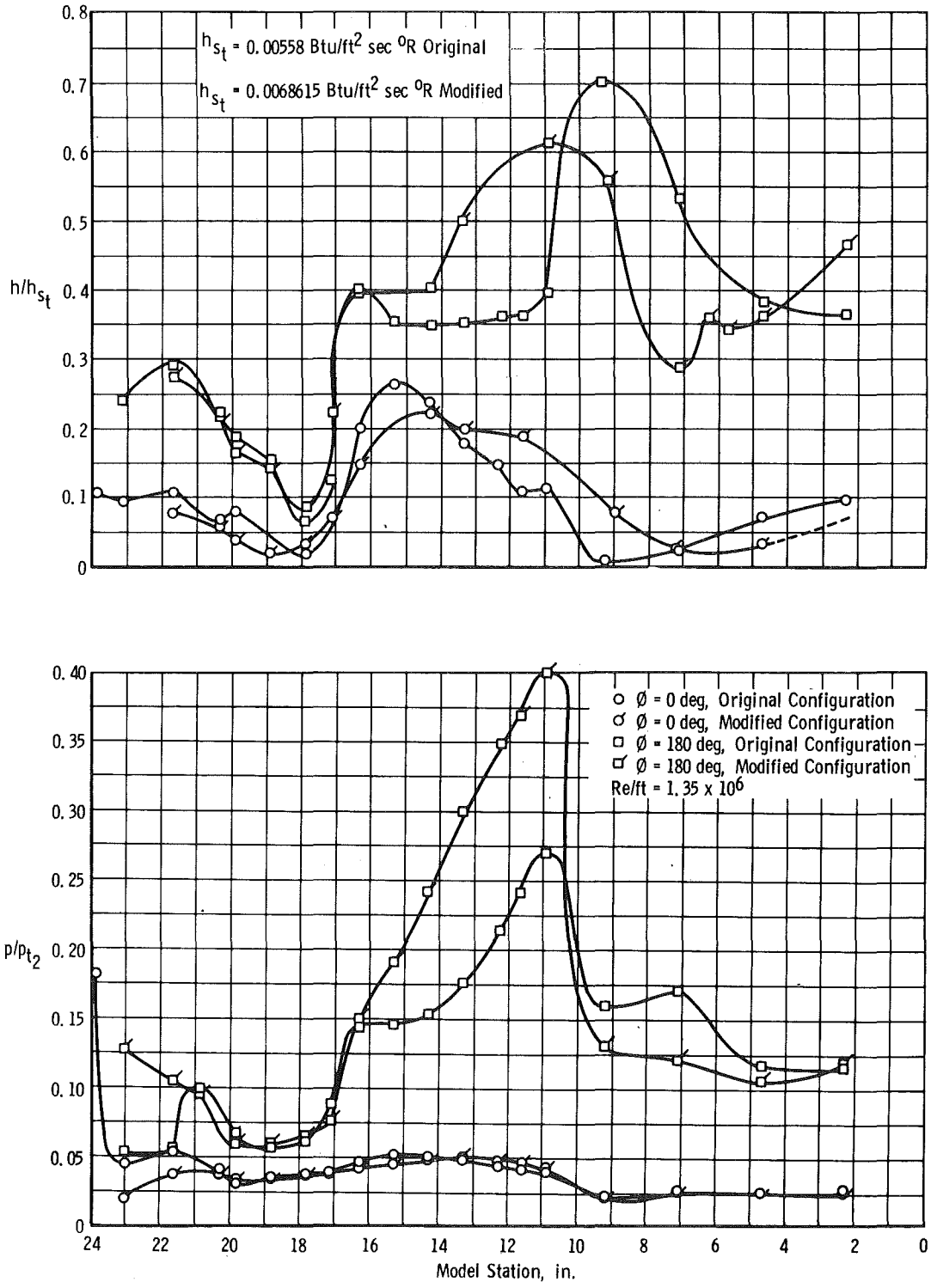

b. α = 10 deg

Fig. 9 Continued

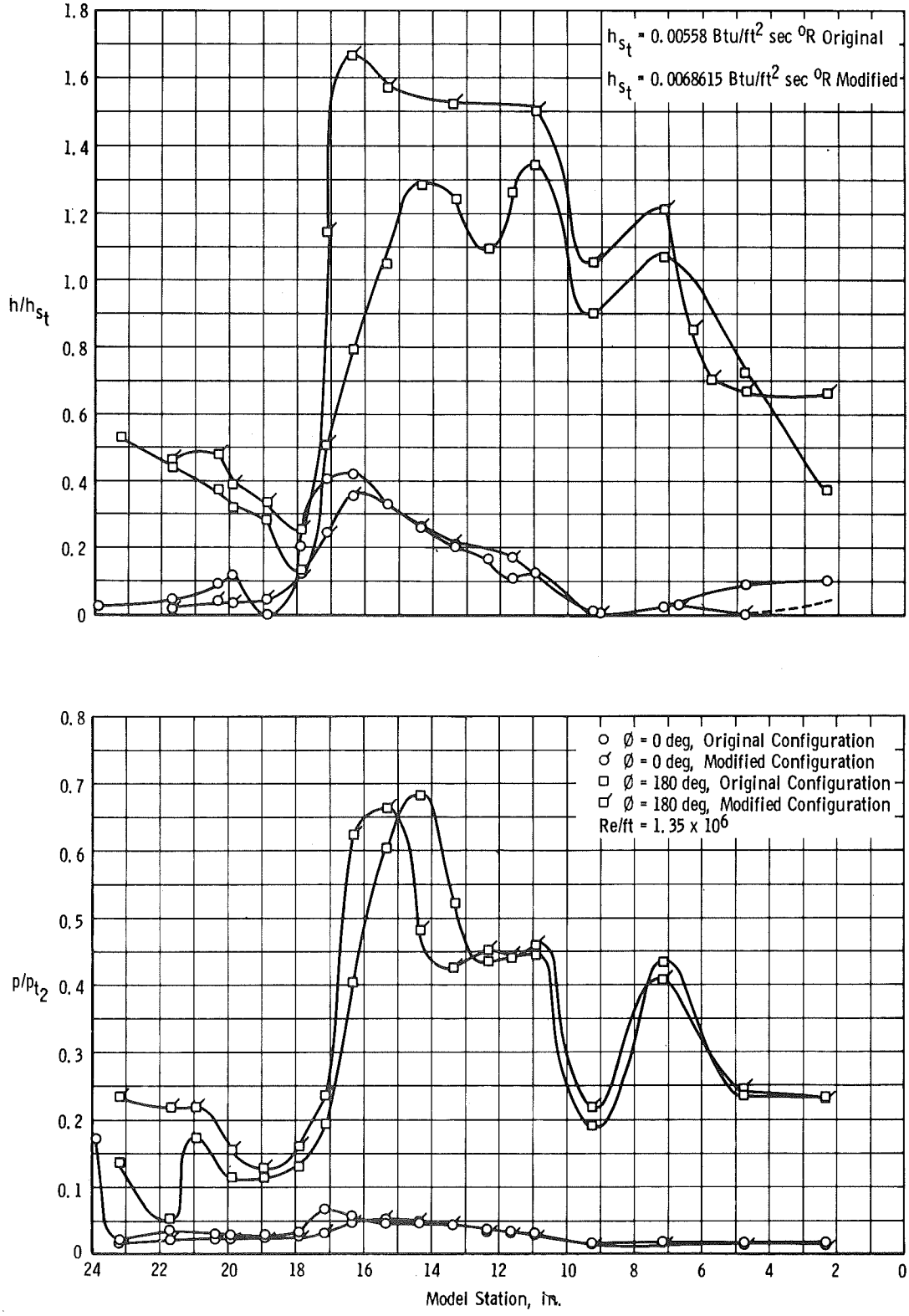

c. α = 20 deg

Fig. 9 Concluded

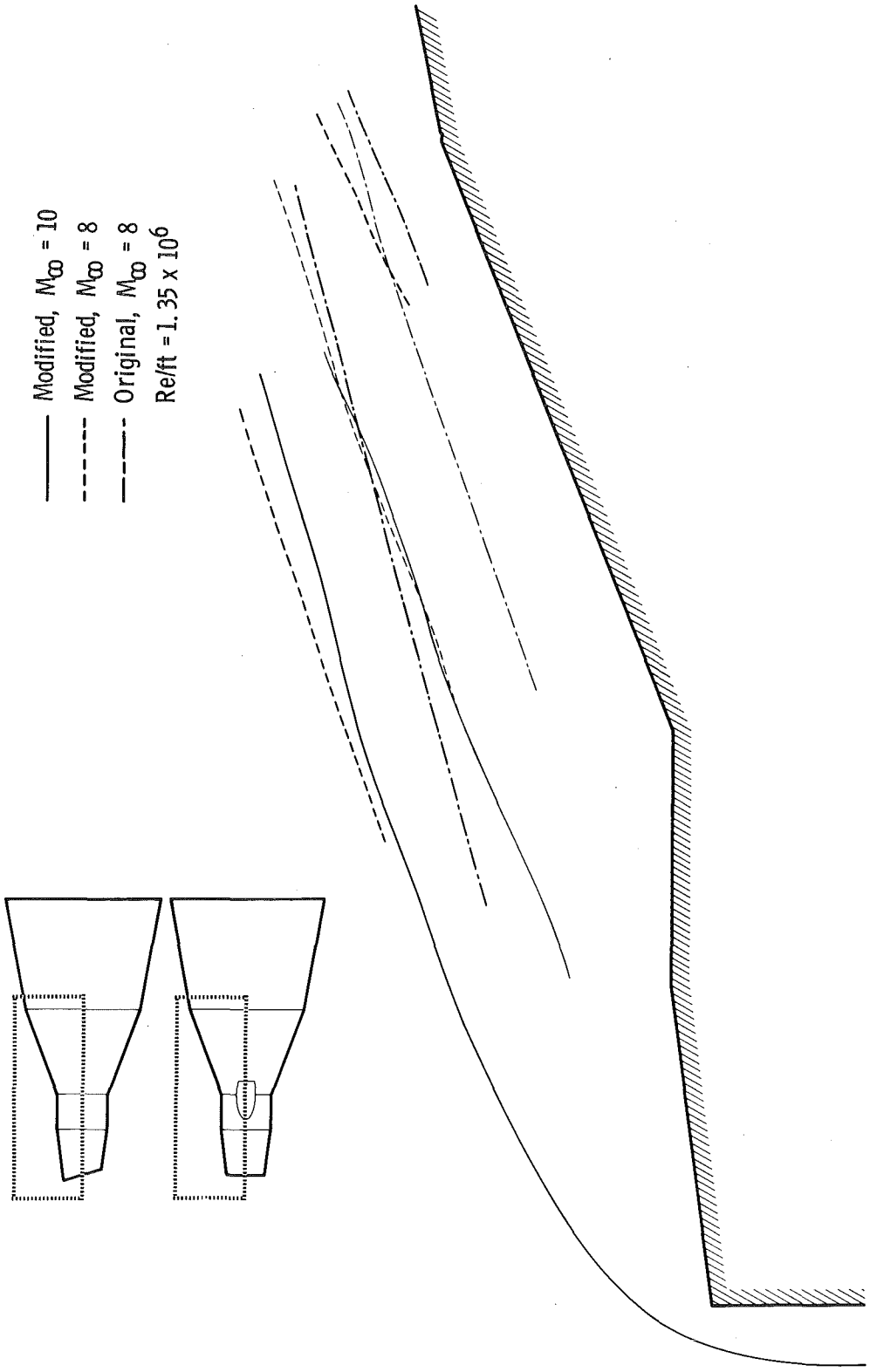

a. $\alpha = 0$ deg

Fig. 10 Composite Sketches of the Flow over the Original and Modified Exit Configurations at Mach Numbers of 8 and 10

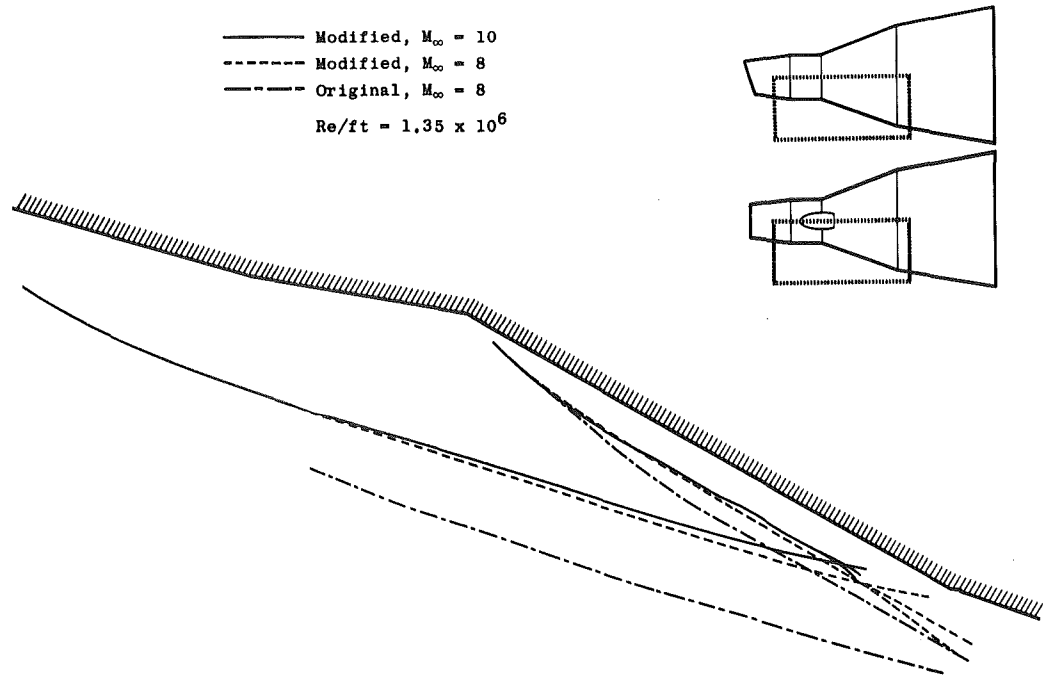

b. α = 10 deg

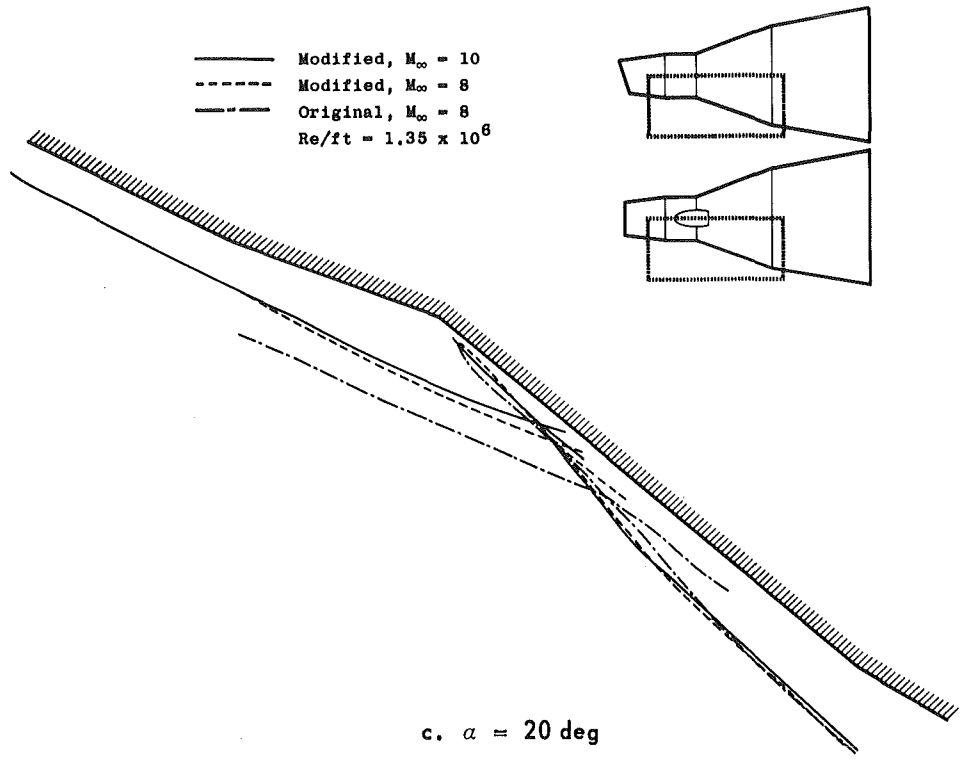

c. α = 20 deg

Fig. 10 Concluded

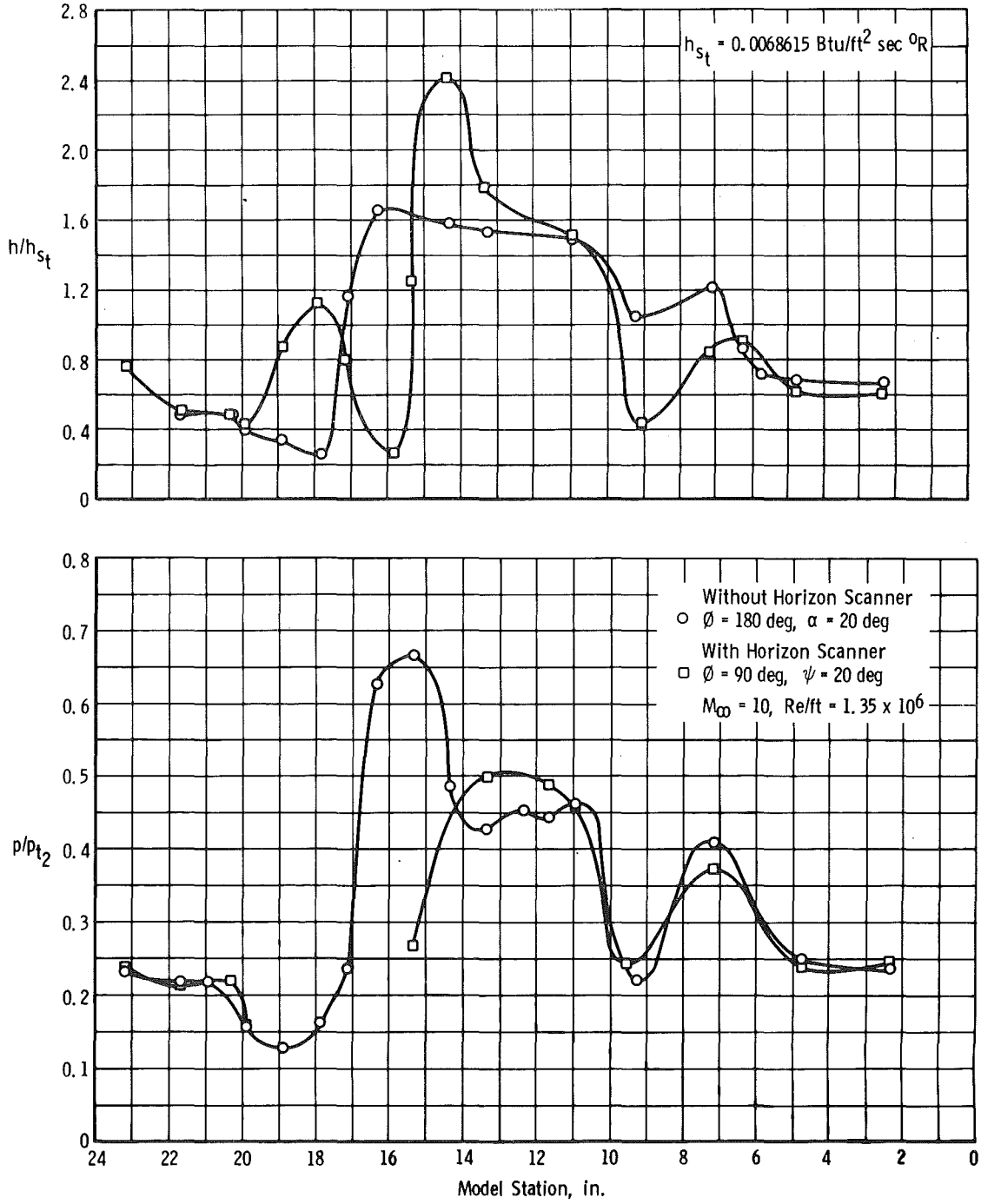

Fig. 11 Comparison of Pressure and Heat-Transfer Distributions on the Exit Configuration, Horizon Scanner Effect

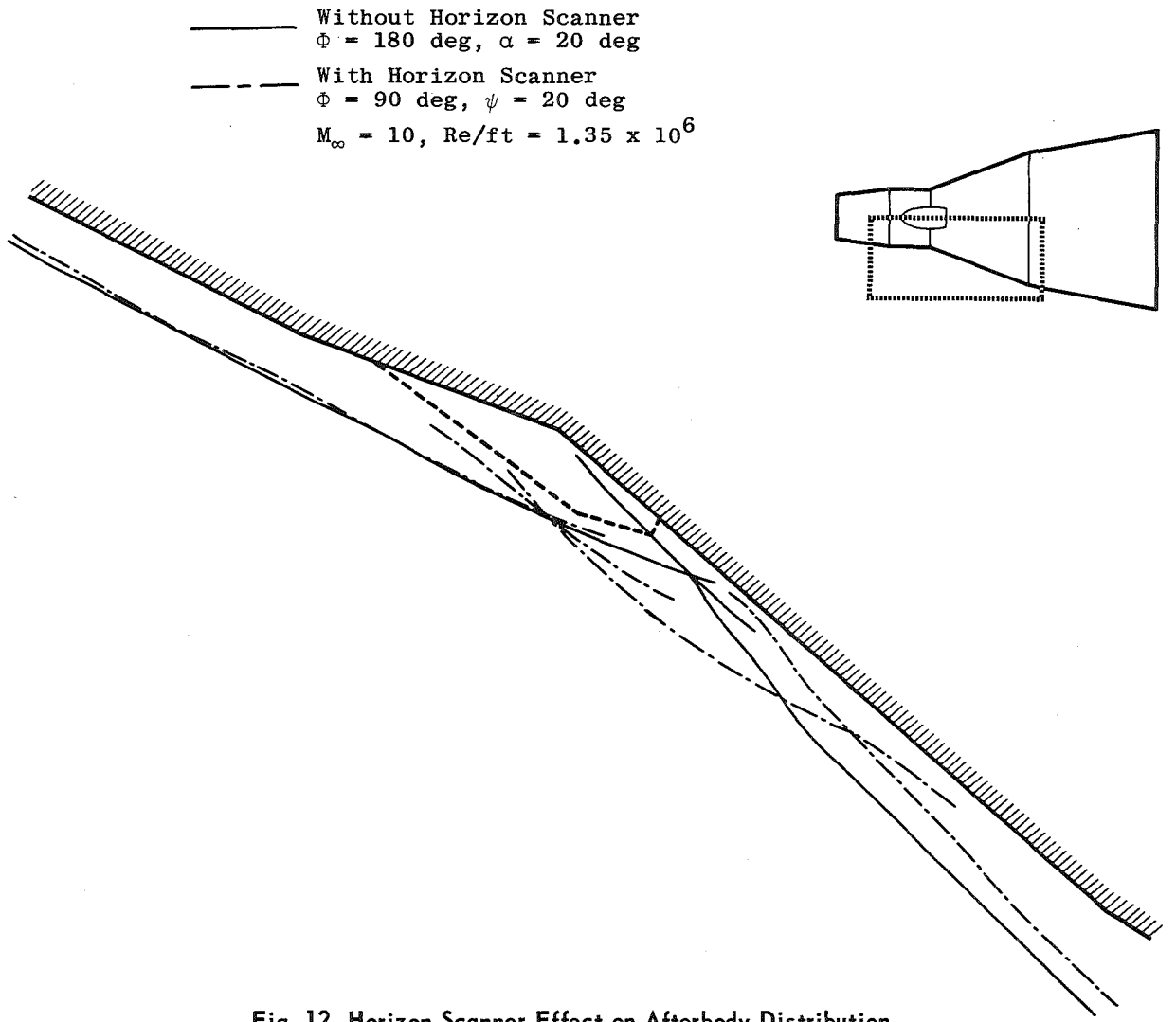

Fig. 12 Horizon Scanner Effect on Afterbody Distribution

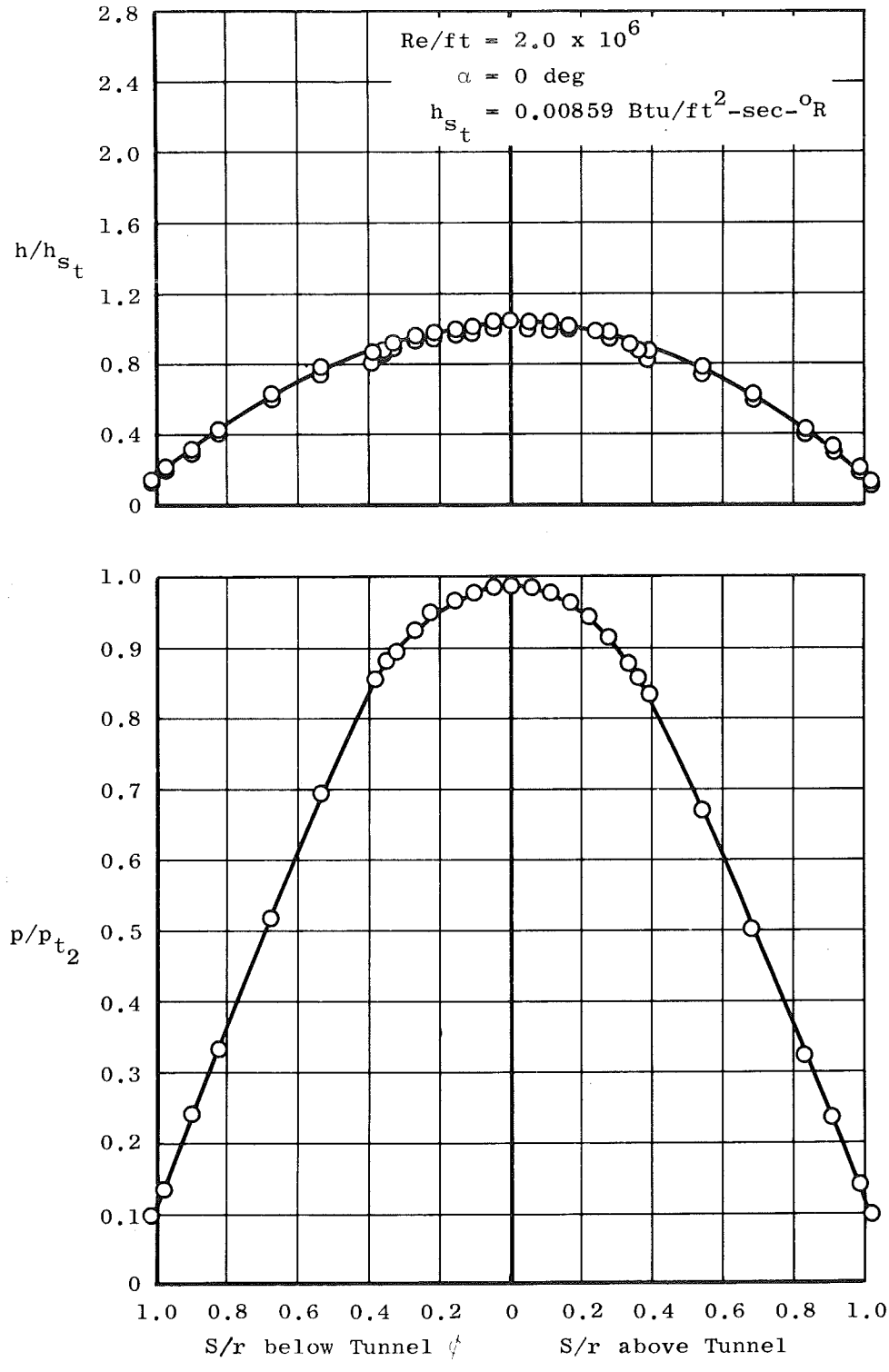

Fig. 13 Pressure and Heat-Transfer Distribution on the Hemisphere-Cylinder

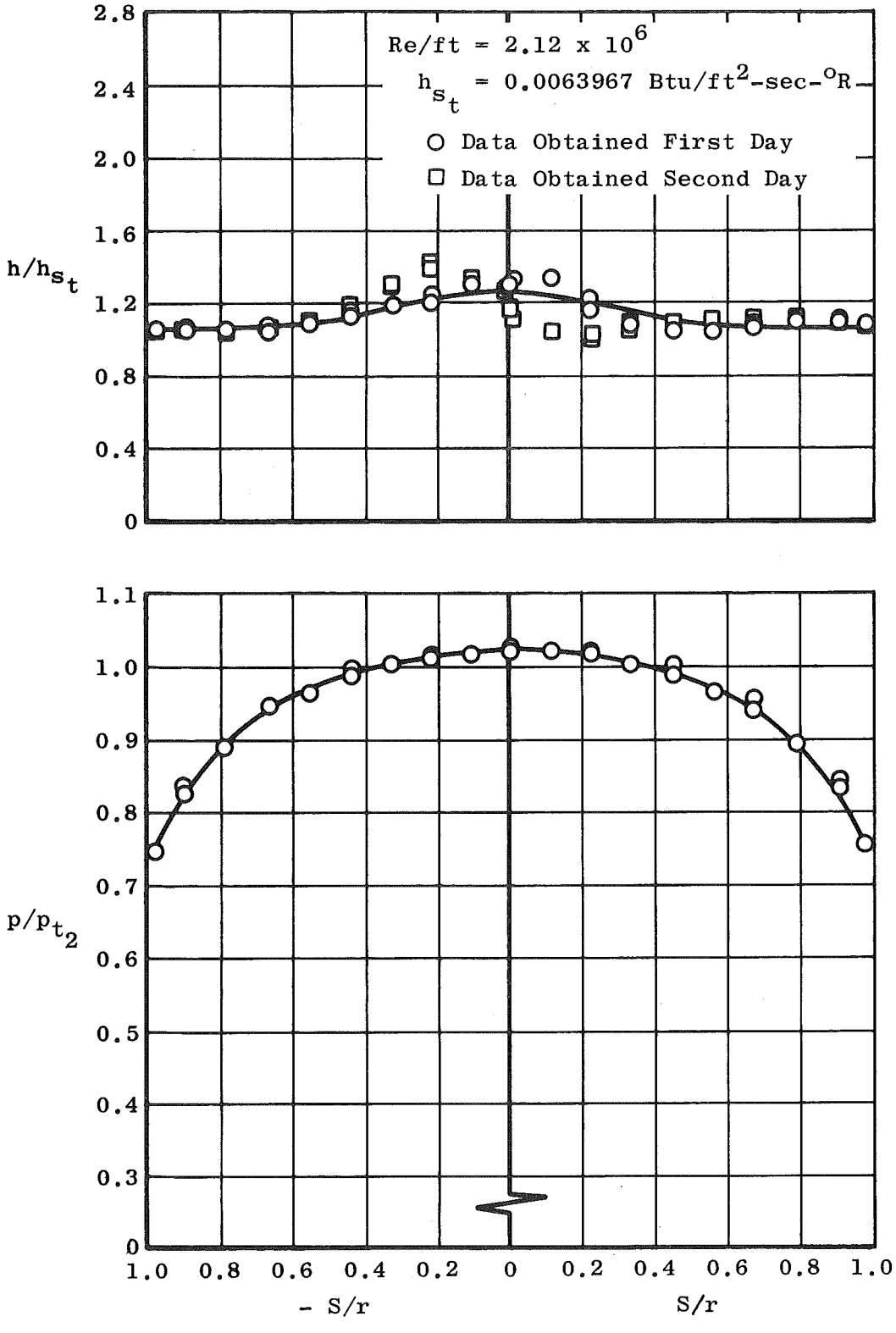

a. α = 0 deg

Fig. 14 Pressure and Heat-Transfer Distribution on the Heat Shield of the Re-Entry Configuration

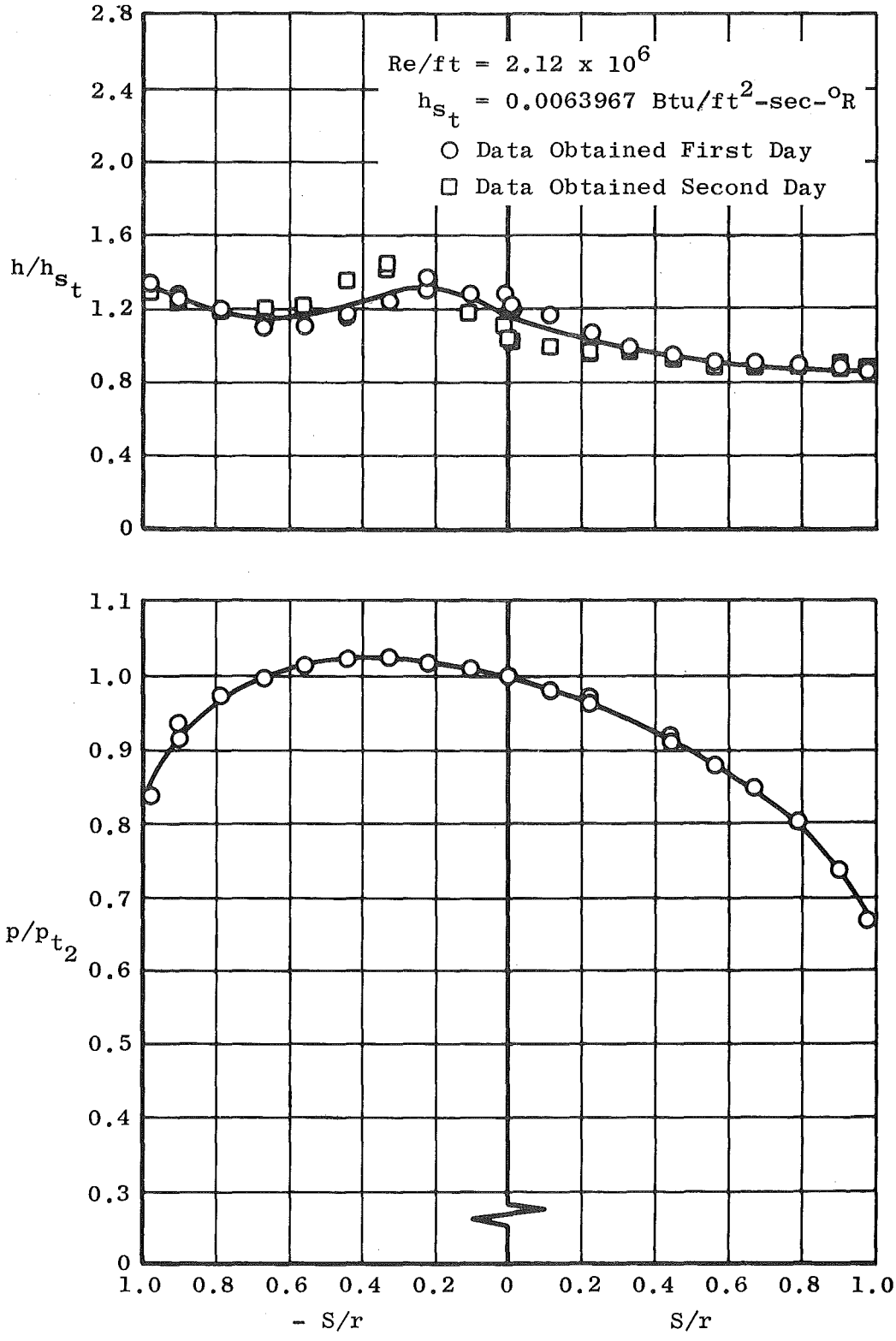

b. α = 10 deg

Fig. 14 Continued

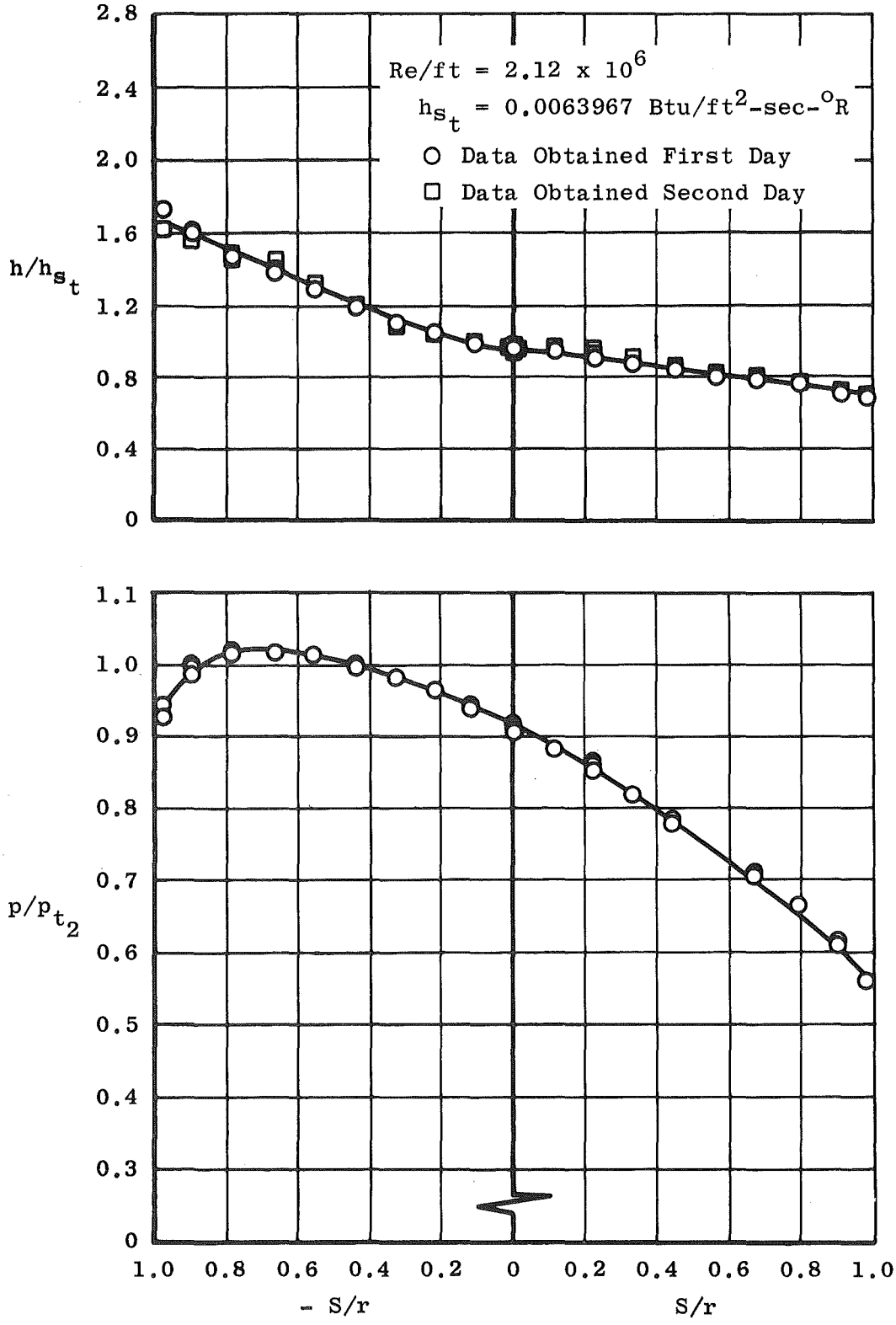

c. α = 20 deg

Fig. 14 Continued

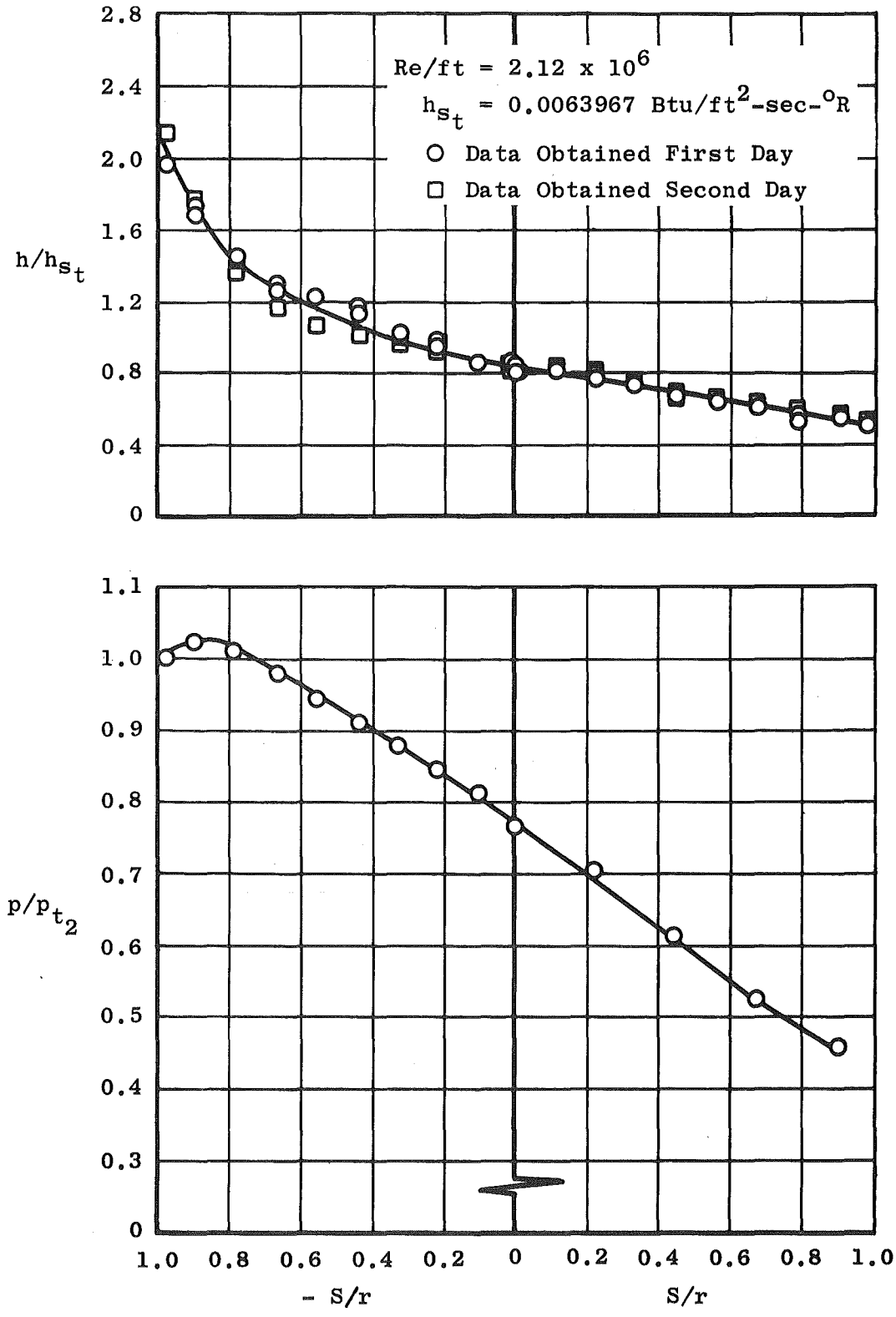

d. α = 30 deg

Fig. 14 Continued

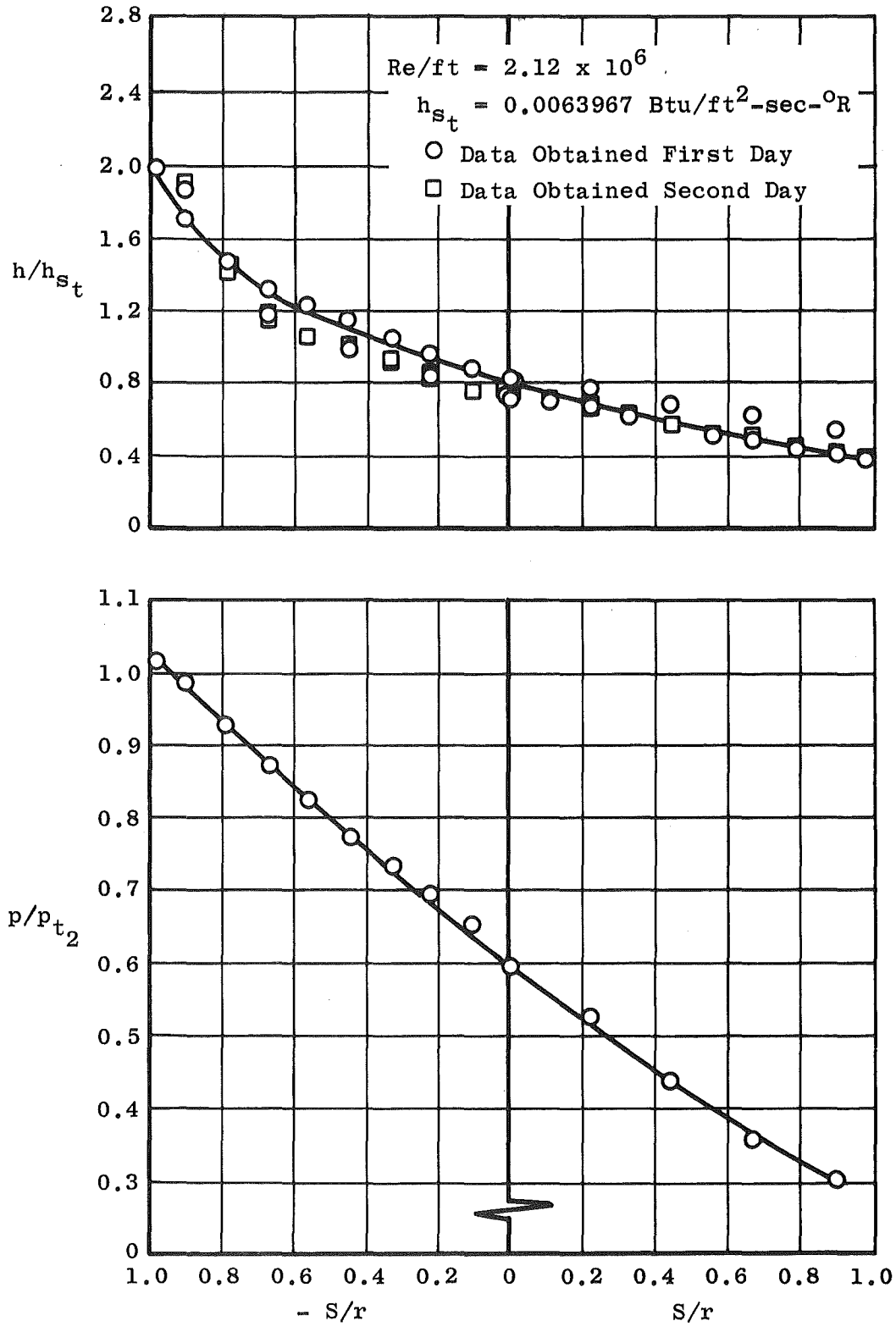

e. α = 40 deg

Fig. 14 Concluded

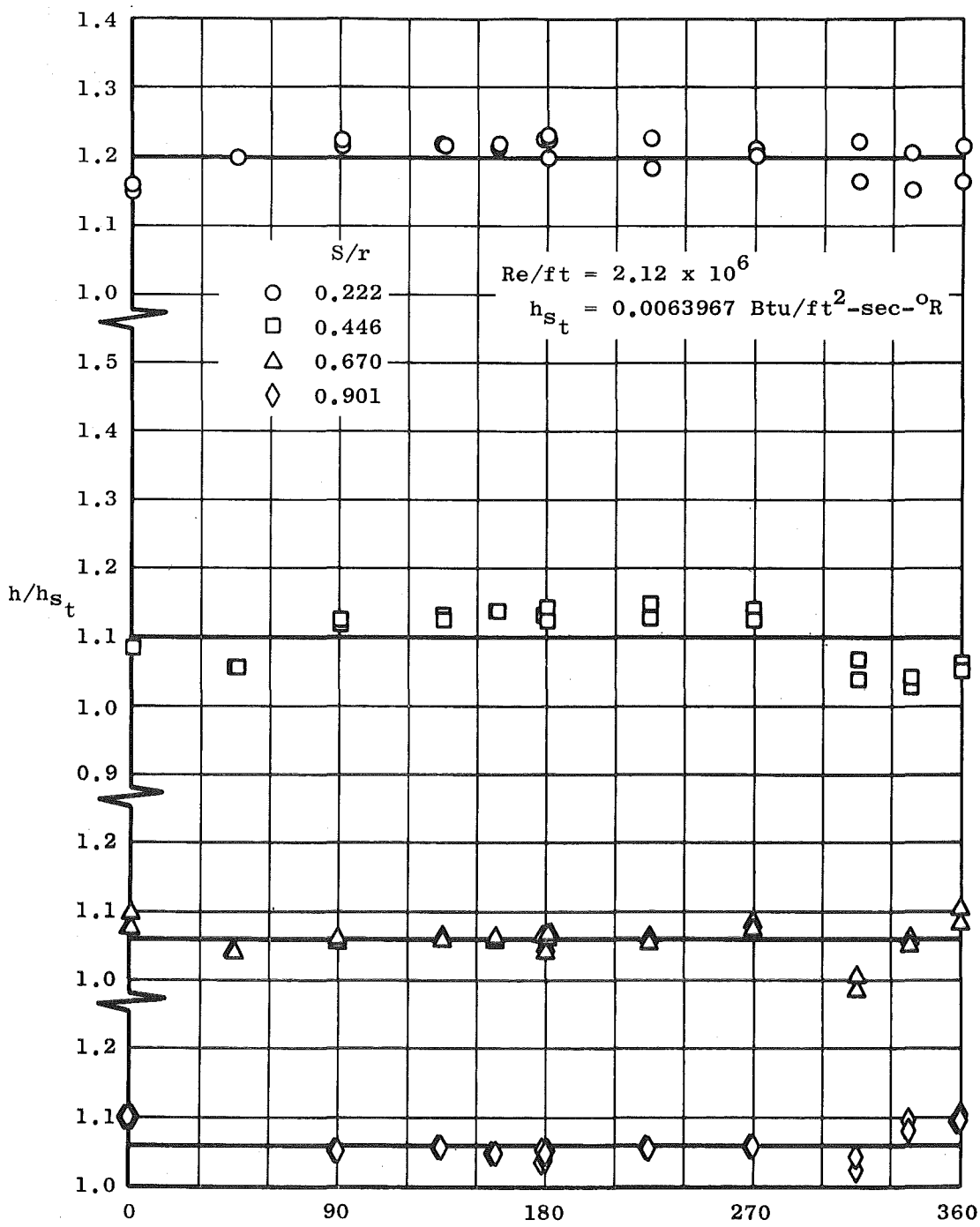

a. α = 0 deg

Fig. 15 Heat-Transfer Distribution on the Heat Shield at a Constant Value of S/S* with Respect to Tunnel Roll Angle

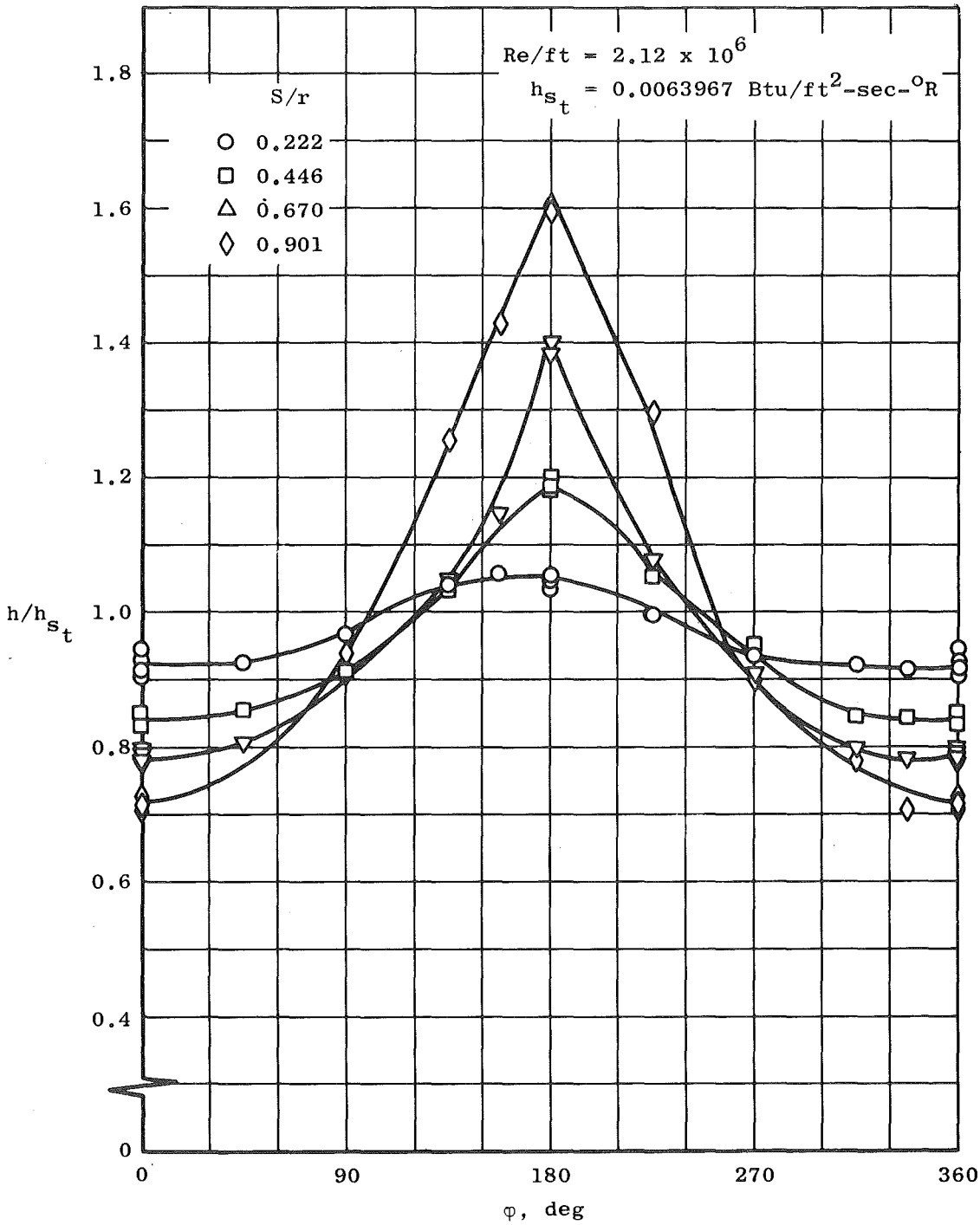

b. α = 20 deg

Fig. 15 Continued

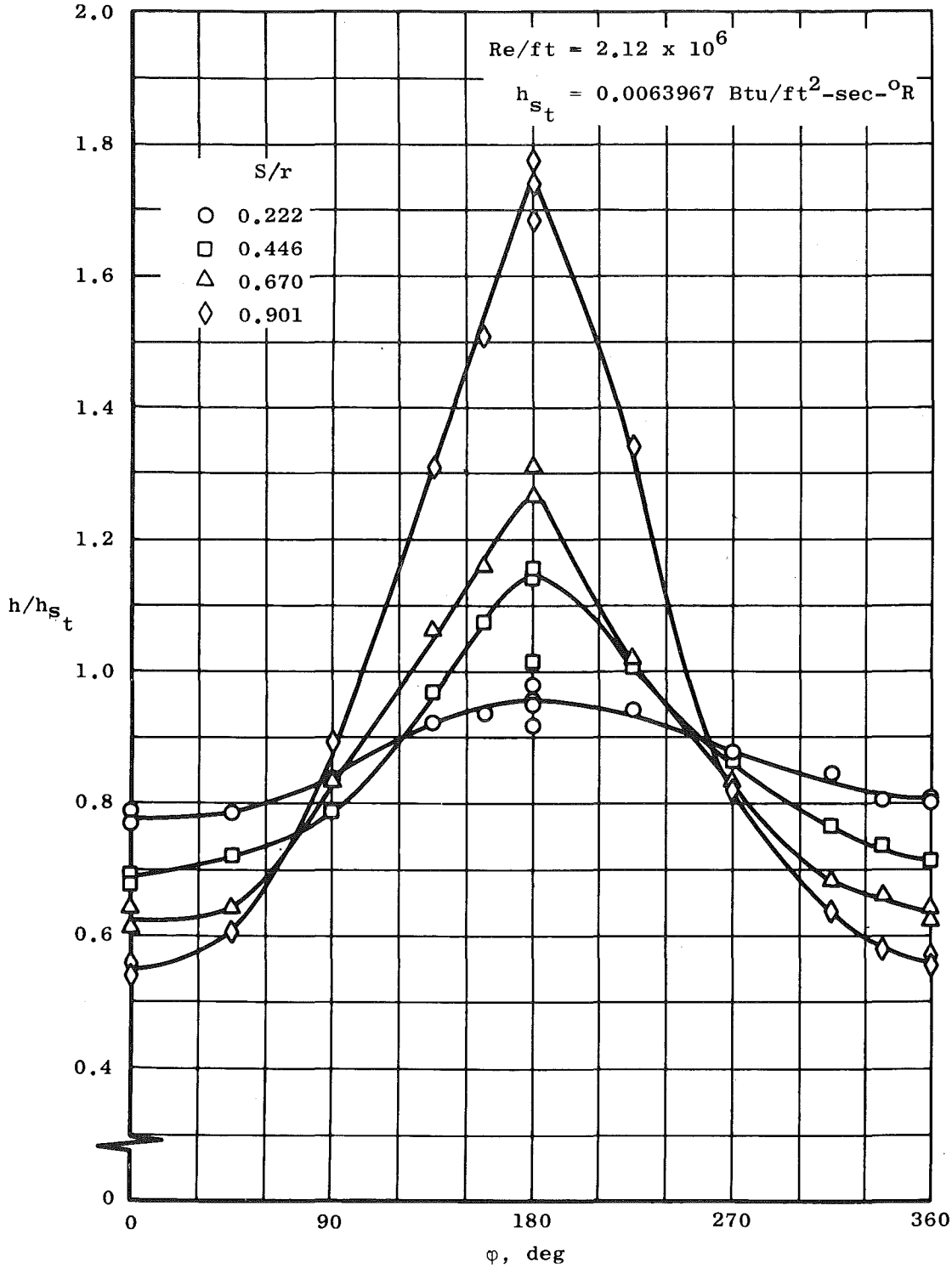

c. α = 30 deg

Fig. 15 Concluded

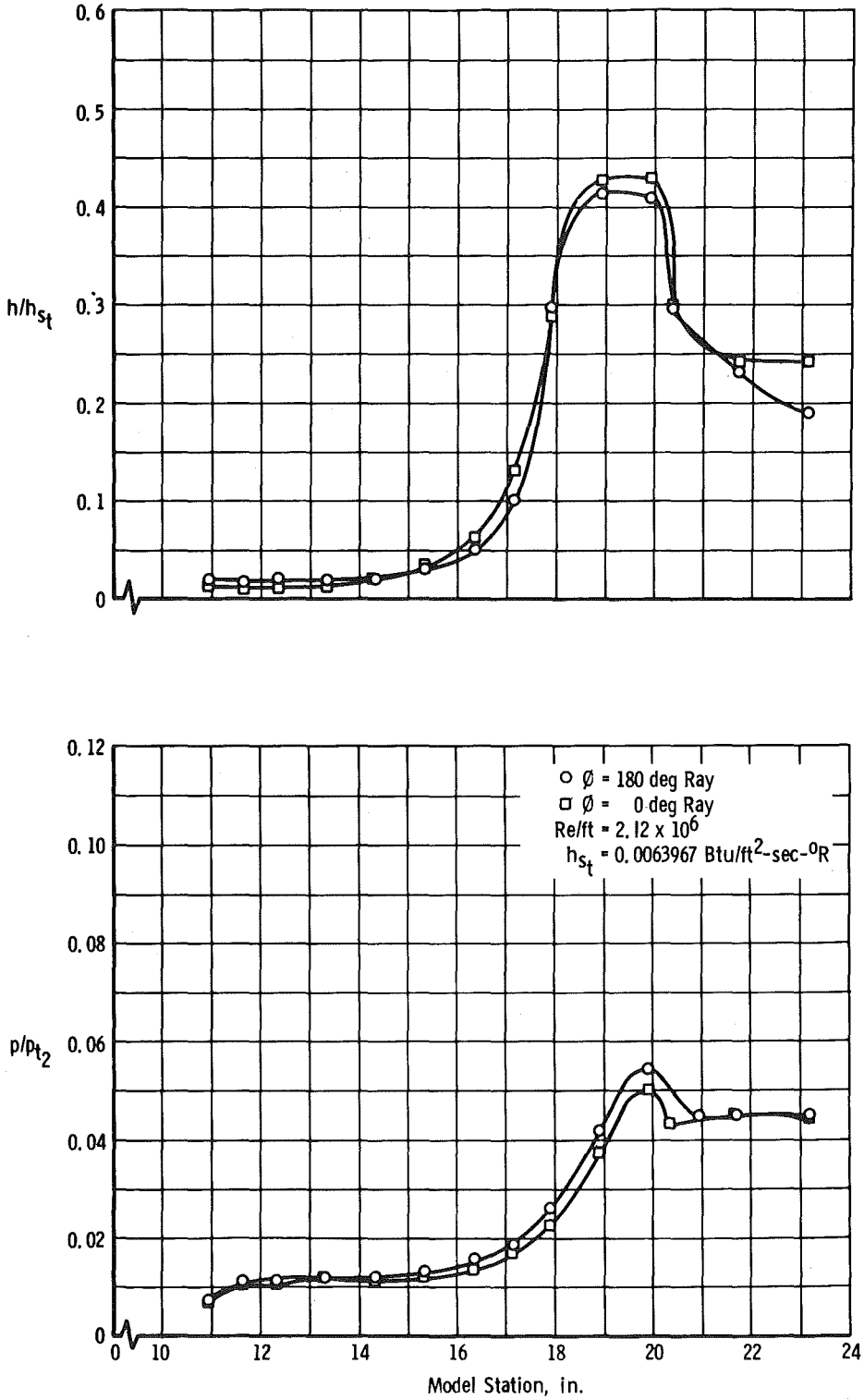

a. α = 0 deg

Fig. 16 Pressure and Heat-Transfer Distribution on the Afterbody of the Re-Entry Configuration

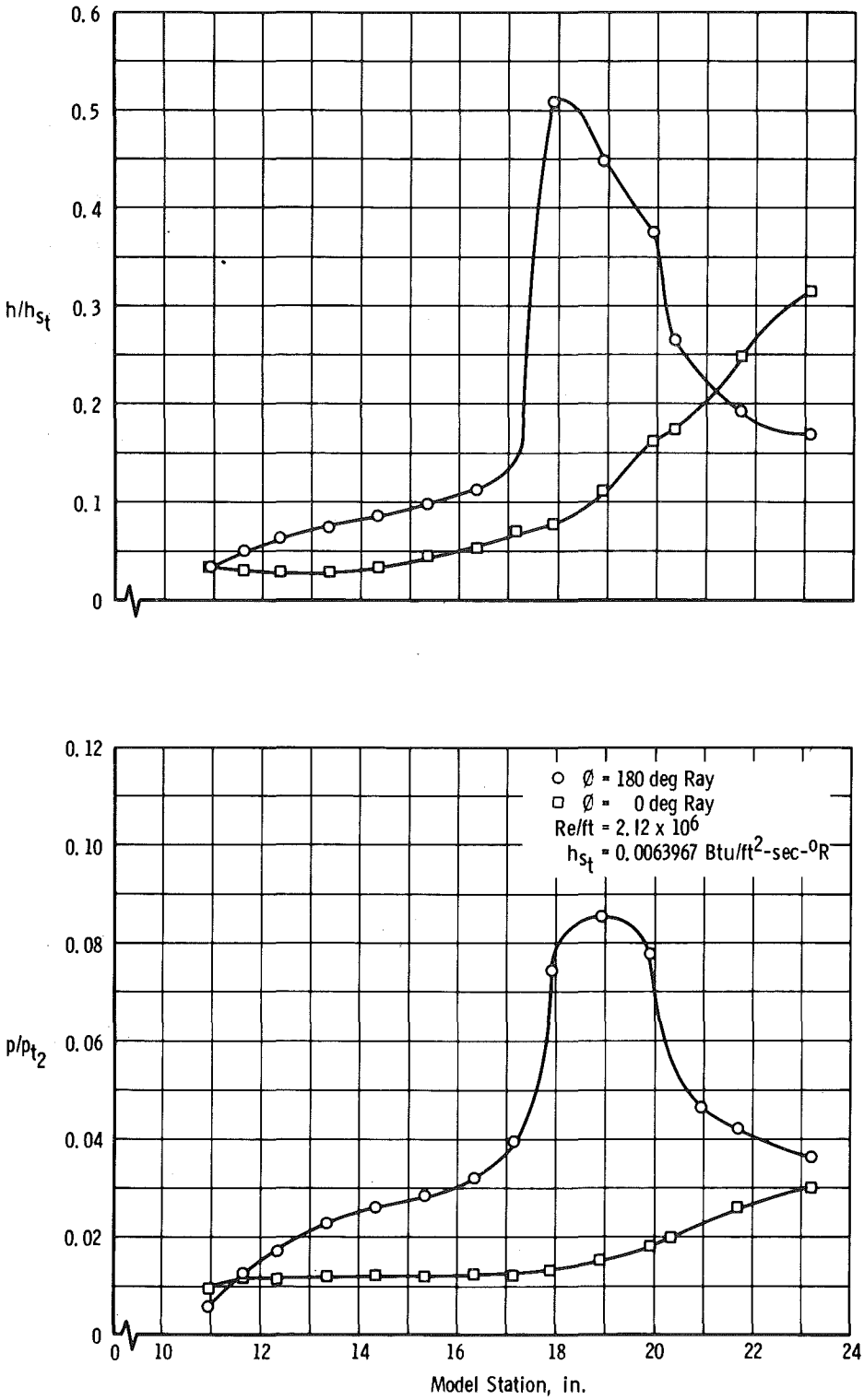

b. α = −10 deg

Fig. 16 Continued

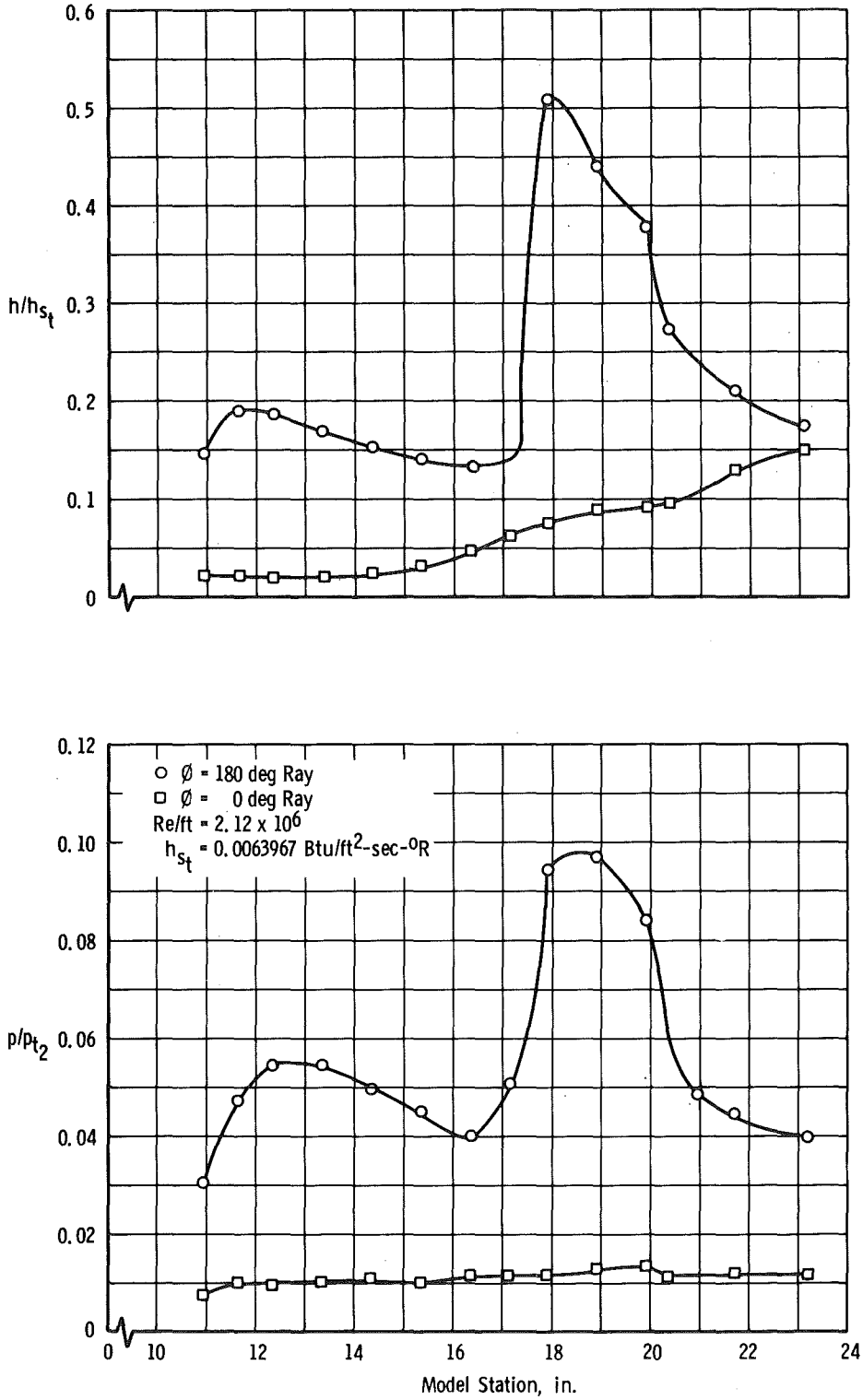

c. α = −20 deg

Fig. 16 Continued

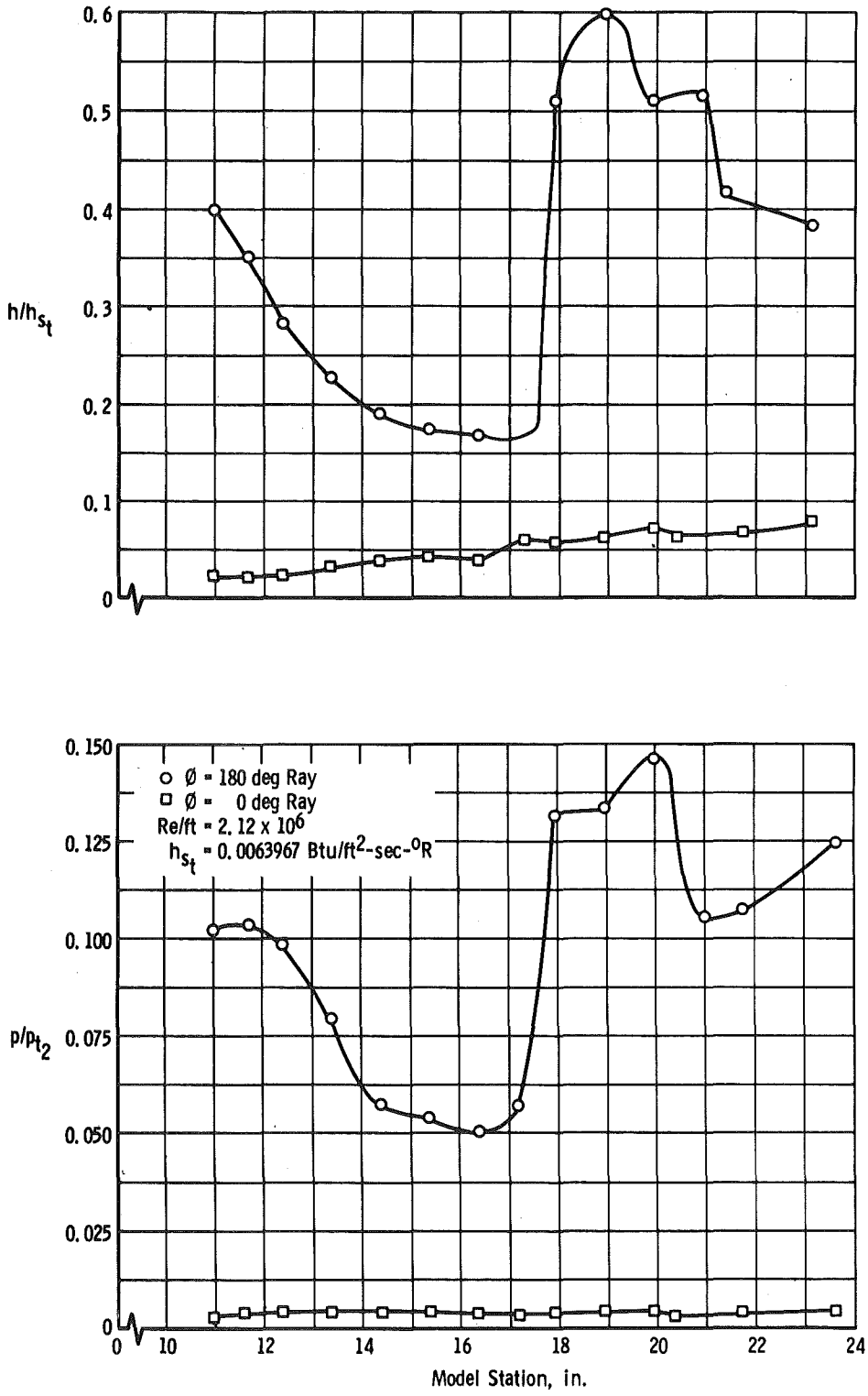

d. α = -30 deg

Fig. 16 Continued

DECLASSIFIED / UNCLASSIFIED

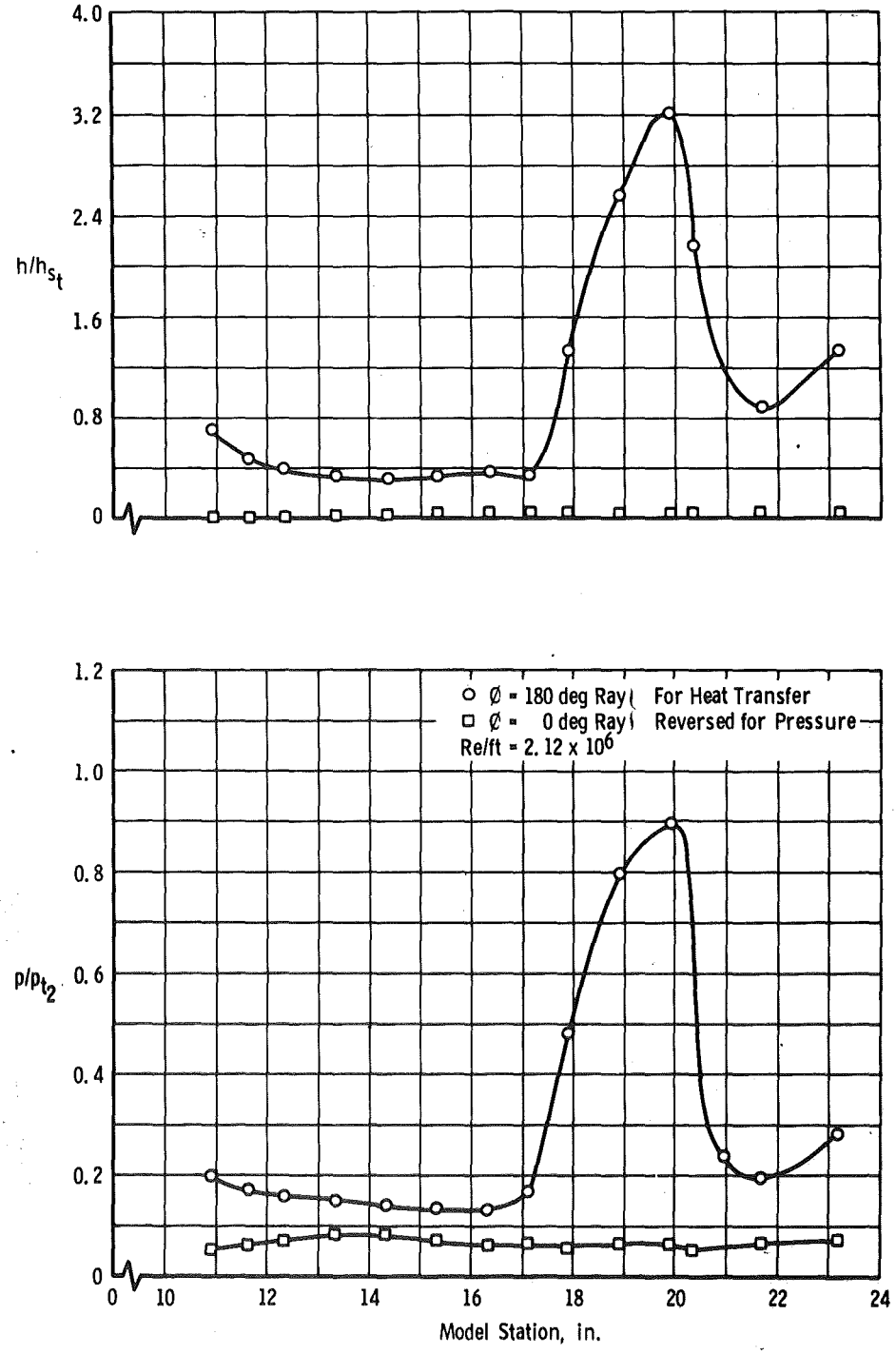

e. $\alpha = -40$ deg

Fig. 16 Concluded

DECLASSIFIED / UNCLASSIFIED